DELFT UNIVERSITY OF TECHNOLOGY

MASTER THESIS

Noninvasive Hemodynamic Monitoring: Left Ventricular Pressure-Volume Loop Reconstruction

Author:
A.L. REDDINGTON

Supervisors:
IR. R. MAESSEN
PROF.DR.IR. R. DEKKER
DR. R.A. BOUWMAN
PROF. DR. H.H.M. KORSTEN

A thesis submitted in fulfillment of the requirements for the degree of Master of Science

in the

Faculty of Mechanical, Maritime, and Materials Engineering

Philips Research Multiphysics and Optics Group

August 8, 2019

DELFT UNIVERSITY OF TECHNOLOGY

Abstract

TU Delft Biomedical Engineering
Faculty of Mechanical, Maritime, and Materials Engineering

Master of Science

**Noninvasive Hemodynamic Monitoring:
Left Ventricular Pressure-Volume Loop Reconstruction**

by A.L. REDDINGTON

Heart disease - already a leading cause of death in industrialized societies - is becoming more and more prevalent as society ages. With this increase, improvements in diagnosis and monitoring of heart disease are necessary. Current state-of-the-art cardiac assessment techniques are invasive and too strenuous for heart disease patients. Therefore, there is a need for a noninvasive, fast, and mobile cardiac evaluation method. We propose the use of personalized lumped parameter models to simulate the circulatory system, so that left ventricular pressure can be estimated from left ventricular volume as acquired with 3D ultrasound imaging. Subsequently, the estimated pressure and the imaged left ventricular volume can be used to reconstruct pressure-volume loops, which are significantly indicative of cardiac health. As ultrasound is fast, not strenuous, and can be applied from the bedside, this method is suitable for critical care patients.

Contributions

- The left ventricular pressure and volume can be estimated with noninvasive inputs.
- Aortic pressure can be reproduced with a lumped parameter model and a minimal input dataset consisting of diastolic blood pressure (DBP) and systolic blood pressure (SBP).
- Machine learning techniques confirmed a correlation between vascular properties and patients' BMI, age, and gender, and show promise as a noninvasive parameter personalization method.

Acknowledgements

I would like to express my gratitude for the guidance I received from Ralph Maessen, Ronald Dekker, Arthur Bouwman, Kevin Lau, Peter Bingley, Marco Baragona, Onno Wieleman, and Erik Korsten. Thank you for the fruitful discussions about my work. I would also like to thank the Philips Intern Community for making my time in Eindhoven enjoyable.

This project was funded by Philips Research. Data was collected by clinical collaborator Catharina Hospital Eindhoven for own use and was shared with Philips. Ethics committee approval was waived by the Medical Ethics Review Committee (METC) of the Catharina Hospital Eindhoven on the grounds of the study being a non- Medical Research Involving Human Subjects Act (niet-WMO) study (see appendix D). The study protocol was approved by the Philips Internal Committee for Biomedical Ethics (ICBE).

Contents

Chapter 1

Introduction

Valvular heart disease is predominant in developed societies. With a prevalence of 2.5%, it is one of the leading causes of death in these parts of the world[28, 50]. Aortic stenosis (AS) is a major contributor to this number, with 0.2-1.3% prevalence in the population group aged under 65, and 2.5-9.8% in people over 75 years old[27, 28, 50, 51]. Notably, it accounts for almost half of all valvular heart disease in patients over 75 years old[28], making it the most common cause of severe heart disease in elderly patients[25]. As the world population ages, valvular heart disease prevalence is expected to increase considerably[69, 50]. As a consequence, the number of AS patients over 75 years old is estimated to double in the next 50 years[28].

As it becomes even more prevalent, improvements should be made in the diagnosis and monitoring of valvular heart disease, in order to improve prognosis. Evaluation of cardiac function is critical in cardiology in many settings, including the intensive care unit (ICU), the operation room (OR), and from any bedside. Currently available techniques for evaluation require highly invasive methods, such as the catheterization of major vessels, which is often combined with complex medical imaging techniques[24, 19]. These imaging techniques, including MRI and nuclear heart scans, are unsuitable for critical care patients, as they cannot be performed from the beside and are too strenuous. Since many patients with valvular heart disease are critical care patients, this presents an issue. There is a need for a non-invasive, quick, and bedside-suitable evaluation system for cardiac function.

Ultrasound is an imaging technique that is not strenuous for patients and can be used anywhere, including the ICU, OR, and bedside[24]. As it provides information on the geometry of the heart, it could be a good starting point to developing such an evaluation system. For example, left-ventricular volume can be extracted from ultrasound images, from which aortic flow can be obtained. These are important cardiac parameters. A model should then be developed that simulates the circulatory system, so that cardiac function can be assessed with these measures as inputs.

The first step in developing such a model, is determining which cardiac measurements are most informative of cardiac function, so that the model can be designed to output these measurements. In appendix A we find that the goal of our model should be to reconstruct left ventricular (LV) pressure-volume (PV) loops (figure A.1,2,3), as they provide much information regarding left ventricular function, which can be useful in a diagnostic or monitoring context. LV pressure and volume are currently not computed in real-time clinically, as their construction typically requires invasive methods. Noninvasive estimation of PV relations has been studied previously[13, 62, 36], showcasing its feasibility. If a model could be developed that simulates the circulatory system, this would allow estimation of LV pressure from aortic flow recordings

acquired through 3D ultrasound imaging of the left ventricle. Then LV PV loops with exclusively noninvasive inputs could be constructed in real-time, which would be of great benefit to existing heart disease diagnosis and treatment protocols, as more accurate diagnoses could be made in a shorter time frame.

Since vascular properties can vary greatly between patients, a lot of attention should be dedicated to making such a model patient-specific. Throughout this thesis we will develop and evaluate the performance of a patient-specific model that provides a method to reliably assess cardiac function, with exclusively noninvasive cardiac measurements as inputs.

Chapter 2

Methods

Study design In this proof of concept study, we go about testing our model in two phases. The first phase is concerned with testing how well the model can approximate aortic pressure, when the three degrees of freedom in its parameters can be fully optimized to best fit the known aortic pressure, which is acquired invasively with pressure catheters. After confirming that the model is indeed fit to simulate aortic pressure, the next phase includes verifying that the model is useful for estimating aortic pressure, when only offered noninvasive inputs. To demonstrate the feasibility of reconstructing the LV PV loop entirely noninvasively, we validate the outcome of our model against the best fit that the model produced in phase one, as this is the best output that could be reasonably expected. The study protocol was approved by the Philips Internal Committee for Biomedical Ethics (ICBE) and was acknowledged as a non- Medical Research Involving Human Subjects Act (niet-WMO) study by the Medical Ethics Review Committee (METC) of the Catharina Hospital Eindhoven.

Data acquisition Ground truth data for model validation was acquired in the catheter laboratory of the Catharina Hospital Eindhoven, Netherlands during transcatheter aortic valve implantation (TAVI) procedures. The design of the acquisition setup is schematically shown in supp. figure 1[1]. An Epiq 7G 1.5 convex C5-1 ultrasound probe (Philips Healthcare, Bothell, WA, USA) was used to acquire 3D (full volume HVRQ mode) ultrasound images of the LV during ten consecutive beats. Invasive arterial (P1), aortic (P2), and LV pressure (also P2, when the catheter is extended from the aorta into the LV) were measured with a catheter during TAVI. Datex-Ohmeda S/5 Collect software was used for data extraction from the GE Carescape B650 Monitor.

Patients 14 patients were included in the data acquisition phase, of which 8 were male and 6 were female, with an average age of 75.6 $\pm$ 8.51 years (mean $\pm$ STD). They were all patients of the Catharina Hospital Eindhoven who were scheduled for TAVI. Four patients were excluded because either the state of their left ventricle did not allow ultrasound imaging of sufficient quality, or they did not display a regular sinus rhythm.

Data alignment As data was acquired from and stored in different machines (supp. figure 1), their time stamps were not synchronized. To align the data, the ECG signal was stored in all data storage locations and used as an alignment tool. For alignment, the signals were transformed into a more comparable format by finding the intervals between the R waves. The R-R intervals of a short ECG signal from the ultrasound are then slid across the R-R intervals of a longer ECG signal which was measured during the entire procedure, to maximize the R-R interval similarity. The minimal value of a cost function reveals the real lag between the two ECG signals

(figure 1D). Furthermore, when a 3D ultrasound image was made, the time was noted. These times were used as a reference point to verify that the ECG signals were aligned correctly.

Data pre-processing To accurately extract the local optima that represent the R peaks in the ECG signals, the lower frequencies were filtered (high-pass Butterworth filter, cutoff frequency 1 Hz), to allow the R peaks to have a more consistent height. Furthermore, the invasively acquired pressure data were pre-processed, as preliminary results revealed that the systolic blood pressure values of the pressure curves modulated with the frequency of the ventilation (figure 1D). To eliminate this effect, pressure was averaged over multiple beats.

Cardiac quantification Left ventricular volumes were calculated by processing transesophageal echocardiographic (TEE) images with cardiovascular ultrasound quantification software (TOMTEC Arena, TOMTEC Imagin Systems GmbH). For this purpose, the 4D Left Ventricle Analysis application was used and anatomical landmarks were indicated manually in three different views (figure 1B). These are then automatically integrated to form a smooth 3D representation of the left ventricle, of which the boundaries could be manually adjusted if necessary. Reiterating this process for each beat in the image results in an LV volume waveform for ten consecutive beats. Due to the limited quality of TEE images, there is some error introduced into the cardiac quantification. Beat-to-beat and inter-patient differences in image resolution result in varying reproducibility of the cardiac quantification analysis (supp. figure 2). Also, the limited time resolution of TEE ($\sim$13-20 Hz) caused data alignment issues in some cases, which was grounds for exclusion of these data sets.

Model development and personalization A three-element Windkessel model (figure 2B) was chosen as the most suitable model to simulate the circulatory system (see appendix C for reasoning). It takes aortic flow as input and outputs an estimate of aortic pressure. The model was used to derive the differential equations that describe the circulatory system (see appendix B). Aortic pressure was then estimated by solving these equations with non-stiff differential equation solver *ode45* (MATLAB, MathWorks).

Model input

Aortic flow is defined as the derivative of the LV volume waveform, so this can be extracted from the ultrasound images. However, because the acquisition rate of the Epiq 7G is quite low, some physiological characteristics of the volume waveform are lost, including the isovolumetric phases. To reincorporate these features into the volume waveform, we make use of optimization. We assume that the aortic flow should look like an asymmetric half-sine wave given by equation 2.1, and we know that the integral of aortic flow equals the volume waveform. Therefore, we find the optimal extent of asymmetry by fitting the integral of asymmetric half-sines to the volume waveform, where the coefficient of asymmetry m ranges from 0.1 to 0.95, in step sizes of 0.05. Maximal aortic flow is found by dividing the area of the half-sine with amplitude 1 mL/s (that was fit to the volume waveform) by the stroke volume, which can be taken from the volume waveform. The model input is then found by multiplying the fit asymmetrical half-sine by the maximal aortic flow.

$$Q_{aortic} = Q_{aortic,max} * sin(\pi * (t^m)) \tag{2.1}$$

Personalization of the model parameters
For all patients, patient-specific model parameters were found by optimizing (least squares) the model output to best fit the invasively measured aortic pressure curve. The parameters are constrained to physiologically plausible values (R = 0.1 - 2.5, Z = 0.01 - 2.5, C = 0.2 - 2.5). However, to test if the model is still reliable when fed exclusively noninvasive inputs, two noninvasive parameter estimation techniques were investigated. The first method involved minimizing the aortic pressure curve that the model is fitted to, to only diastolic and systolic blood pressure (DBP & SBP). The parameter values were then, once again, found by optimizing them with least squares to fit DBP and SBP. Subsequently, the difference between the maximum of the model output and SBP was subtracted, to place more emphasis on estimating the correct SBP value. In the alternative method, patient-specific model parameters were estimated with a nearest neighbors inspired machine learning algorithm. This estimates a patient's parameters by averaging the known parameters of patients that most likely have similar vascular properties as the new patient, weighted by the likelihood of vascular similarity. This likelihood was calculated by taking the following patient information into consideration: Age, BMI, and gender. The training group consisted of the all the patients whose parameter values were found by optimizing the model output to fit the invasively measured pressure data. The measure of similarity was normalized to expected population values for age and BMI. Only patients who were within a certain similarity range defined by radius R from the patient whose parameters were being estimated, were included in the weighted average. R ranged between 0.01 and 0.2.

LV PV loop reconstruction The LV PV loop is found by plotting the LV volume on the x-axis and the estimated aortic pressure on the y-axis.

LV pressure
Since aortic pressure only approximates LV pressure during systole, the model output outside of this phase is not used for PV loop reconstruction. The PV loop is then completed with vertical line segments following the assumption of a great pressure drop or rise during isovolumetric phases. The diastolic filling segment of the pressure curve is outside of the scope of this work, so the PV loop is extended until the x-axis.

LV volume
The LV volume used in reconstructing the PV loop is the integral of the aortic flow curve that was found by optimizing an asymmetric half-sine to the raw LV volume data taken from the ultrasound images, as described in the *model input* section.

Model validation & Statistics To validate the use of the 3EWK model to simulate the circulatory system in general, we compare its output to invasively measured aortic pressure, when its parameters are optimally fitted to these same data. Since only the pressure during the systolic phase is used for PV loop reconstruction, the rest of the curve is excluded from this comparison. We quantify the performance of the model through the mean average error of the model output during systole, combined with the Spearman correlation of the model output and the measured data. To validate subsequent parameter estimation methods, a similar approach

is implemented. However, in this case the model output is not compared to the invasively measured aortic pressure, but to the optimally fitted model output, as this is the best performance that could be reasonably expected from the model.

Chapter 3

Results

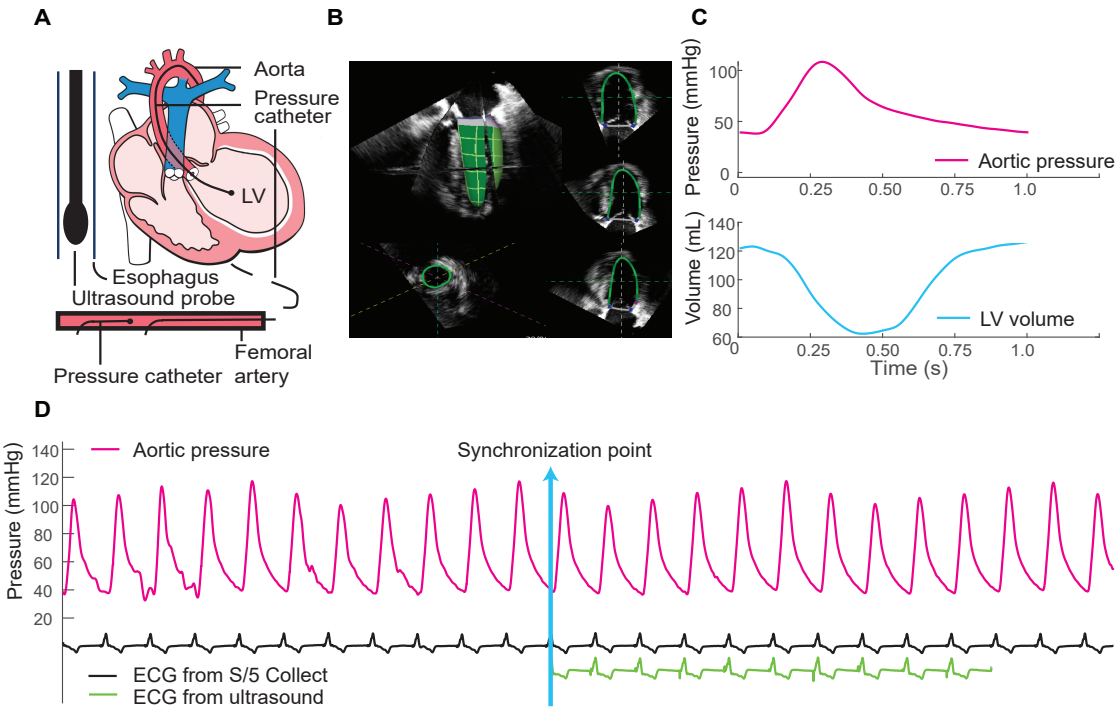

Figure 1. Experimental setup for data acquisition

A The acquisition setup. (Figure adapted from [1]). Ultrasound images were taken via the esophagus (TEE). Aortic and femoral pressure were measured with pressure catheters in their respective arteries. Before and after placement of a new aortic valve, the catheter in the aorta is moved into the LV, providing a short measurement of LV pressure. **B** The ultrasound images are processed with cardiac quantification software (TOMTEC Arena, 4D Left Ventricle Analysis). The boundaries shown in green lines in four different views are integrated to form a 3D representation of the LV volume over 10 beats. The boundaries can be adjusted separately for each beat. **C** An example of the measured signals for one beat (raw data). Aortic pressure is given in fuchsia and LV volume is given in blue. **D** An example of the use of ECG signals for synchronization of two time series. The large ECG recording that is measured throughout the procedure continuously (and is saved into S/5 Collect) is shown in black, whereas the short ECG recording that is taken in parallel with the ultrasound image is given in green. We see that the R peaks of these signals are aligned, showcasing their synchronicity. The point of synchronization indicates the lag that was found between the two measurements. Above the ECG signals, aortic pressure is given in fuchsia. We see that the local maxima of the aortic pressure modulate with a sine wave.

We propose the use of the three-element Windkessel (3EWK) model to simulate the circulatory system (figure 2B, for reasoning see Appendix C). This model is a lumped parameter model: a type of model that decomposes a physiological system into elementary physical components that follow established physical laws, so their relationships can be expressed by simple mathematical equations. In our case, the circulatory system is modelled as an electric circuit. This circuit includes a current source, which simulates the heart pumping blood into the system, where blood flow

is modelled as current; a resistor, which simulates the resistance to blood flow largely due to the capillaries; a capacitor, which represents the elasticity or compliance of the vessels; and an impedance, which models the afterload that the LV must overcome during a contraction. As a result of the circuit topology of the analogue electric circuit that follows from this, the governing differential equations of the model can be derived (appendix B), which can be solved to estimate the aortic pressure.

Since the objective of this study is to reconstruct PV loops, the aim of using a model is to estimate LV pressure, whereas the 3EWK model is only suitable to estimate aortic pressure. However, during systole, aortic pressure approximates LV pressure (figure 2A), so that the model output during this phase can be used to reconstruct PV loops, whereas the bottom boundary of the PV loop is outside of the scope of this work (supp. figure 1A).

Validation is a critical step in model development. The performance of a model of the circulatory system must be determined by comparing its output to true, measured data. Since the objective of developing a personalized model of the circulatory system is to provide a reliable noninvasive cardiac assessment method based on the pressure and volume in the LV, an experimental setup was designed so that these signals could be obtained for validation (figure 1A). In particular, aortic pressure should be acquired, as this is the desired output of the model. Transcatheter aortic valve implantation (TAVI) procedures provide an opportunity to collect these data. During TAVI procedures, the aortic and arterial pressure is continuously measured with pressure catheters inserted in the proximal aorta and femoral artery, respectively. Furthermore, as patients are generally anesthetized, a transesophageal echo (TEE) probe can be inserted to image the LV (figure 1A,B). With the use of cardiac quantification software (figure 1B), LV volume can be extracted from these ultrasound images (figure 1C). In this case, 3D ultrasound images were taken of 10 consecutive beats at a time. To ensure that the separate signals were aligned in time, the ECG signal that was stored in the ultrasound image was compared to the ECG signal that was measured continuously during the entire procedure were synchronized (figure 1D).

Aortic flow - equal to the change in LV volume over time - is extracted from the ultrasound images and fed to the 3EWK model as input (figure 2C). Subsequently, the model parameters are fit to the invasively measured aortic pressure data, using a least squares approach. We see that the 3EWK is indeed suitable for modelling the circulatory system, and can output an accurate estimation of aortic pressure, when fed aortic flow as input (figure 2D,E,G,H). Averaged over all patients, pre-TAVI, the model could predict aortic pressure with 4.6 mmHg accuracy (Spearman correlation = 0.9720), and post-TAVI, the average output error became 3.3 mmHg (Spearman correlation = 0.9548) (figure 2F,I). These discrepancies between measured data and modelled pressure are likely a result of TEE having a relatively poor time resolution ($\sim$13-20 Hz), so that the volume and pressure curves are not exactly aligned in some cases.

We also found that the model has large adaptability (supp. figure 4), meaning that it is suitable for use in a large range of physiological states. For example, in one case, a patient was given adrenaline post-TAVI, resulting in a steep rise in blood pressure. Since one of our model assumptions is that parameters R, Z, and C are constant, the rise in stroke volume due to the adrenaline - which is reflected in the ultrasound

image - should account for this pressure change in the model. Indeed, the model could represent this behavior, as the optimal fit follows the raw data faithfully during systole (supp. figure 3B). The optimal parameter values changed by a conservative 10.6%, which is likely a result of the uncertainty introduced by the quality of TEE imaging (supp. figure 2).

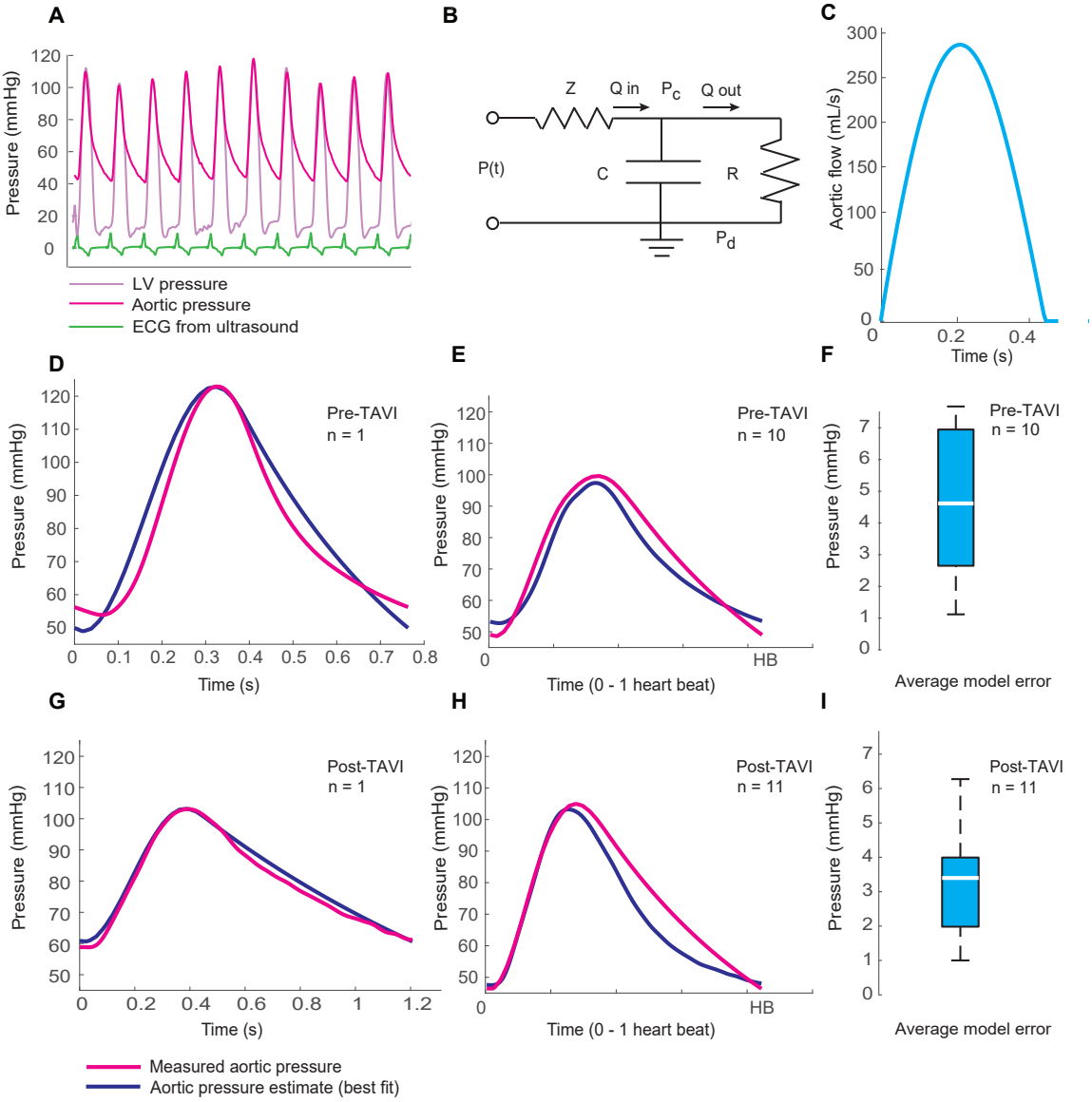

Figure 2. The three-element Windkessel model is suitable for modelling aortic pressure

A During systole, aortic pressure approximates LV pressure. LV pressure is shown in lilac, aortic pressure in fuchsia, and the ECG is given in green. **B** The electric circuit that represents the circulatory system under the assumptions of the 3EWK model. The current source simulates the heart as a pump, where current represents blood flow (Q). The resistor (R) models the resistance to flow provided by the capillaries, the capacitor (C) represents the elasticity or compliance of the vessels, and the impedance (Z) models the aortic afterload. **C** An example of the input for the 3EWK model. Aortic flow, which is taken from the ultrasound images, is fed to the model as input. **D & G** An example from one patient of the aortic pressure estimated with the 3EWK model (dark blue) compared to the aortic pressure measured with a catheter (fuchsia), pre-TAVI (**D**) and post-TAVI (**G**). Here, the model parameters have been optimally fit to the measured data. **E & H** The mean average aortic pressure estimation of all patients, summarizing the performance of the optimal fit of the model, pre-TAVI (**E**) and post-TAVI (**H**). On average, the optimal fit of the 3EWK model performs with an error of 4.6 mmHg pre-TAVI (**F**) and 3.3 mmHg post-TAVI (**I**).

Parameter estimation with a minimized pressure data set

No relevant meaning can be inferred from the model that we have been discussing if it does not represent patient-specific physiology. As such, the determination of the parameters of the 3EWK model must be reiterated for each individual patient. In the above section, patient-specific model parameters were found by fitting the model output to the invasively obtained real aortic pressure. However, to allow clinical applicability, the parameters must be estimated with noninvasive methods, as the pressure curve is not known for patients who need to be diagnosed or monitored in the clinic.

While noninvasive arterial blood pressure estimation methods reconstructing the entire arterial pressure waveform are generally insufficiently reliable[57], there are many noninvasive techniques that do show a promising accuracy in estimating diastolic (DBP) and systolic blood pressure (SBP) [18, 14]. Methods include a wide range of techniques, such as vascular unloading with finger cuffs, for example, the Finapres NOVA (Finapres Medical Systems) and ClearSight (Edwards Lifesciences)[2]. Other methods rely on photoplethysmography[77, 34, 52], Doppler imaging[22], heart sound analysis[30], and ballistocardiography[78]. Micro-scale wearable devices have also been developed widely, mostly based on piezoelectric-induced sensors measuring pulse transit time (PTT) [43, 60, 35], where some are assisted by machine learning techniques [26, 34]. Of course, let us not forget the most widely implemented noninvasive arterial blood pressure estimation method: Oscillometric blood pressure monitoring with a cuff on the upper arm [53, 46]. This last method is well integrated into hospital procedures globally, making it an excellent source of input that we could make use of in our model. Therefore, we investigated whether the 3EWK model could still provide an accurate estimation of the aortic pressure curve during aortic flow, when the data it fits its parameters to is minimized to just DBP and SBP.

In figure 3 we see that the aortic pressure can indeed be estimated accurately with just this minimal data set, which only includes information that can be measured noninvasively. Both before and after TAVI, this estimation method was successful in all patients. On average, when only the minimal data set was fed to the model, the output displayed an error of 0.80 mmHg (Spearman correlation = 0.9996) pre-TAVI, and an error of 1.6 mmHg (Spearman correlation = 0.9950) post-TAVI, when compared to the optimal fit of the 3EWK to invasively measured aortic pressure (figure 3F).

Parameter estimation through machine learning

Still there is much debate over the reliability of the noninvasive DBP and SBP estimation methods mentioned above[79, 67, 72]. Therefore, we developed an alternative parameter estimation method, which is independent from any pressure measurements, be it noninvasive or invasive. To achieve this, machine learning techniques were implemented. The patients for which the true pressure curve is known - and for which the model parameters can be found with the aforementioned techniques - function as a training group on which we learn a model that predicts the parameter values for future patients. A nearest neighbors-inspired algorithm was developed, which determines the probable vascular similarity between the sample group patients and a new patient (figure 4, panel A & B). This method relies on the fact that vascular properties and patient properties - such as their age[76, 40, 39, 31], BMI[63, 73, 29, 47], and gender[64, 42, 4, 45, 15] - are related, which has been

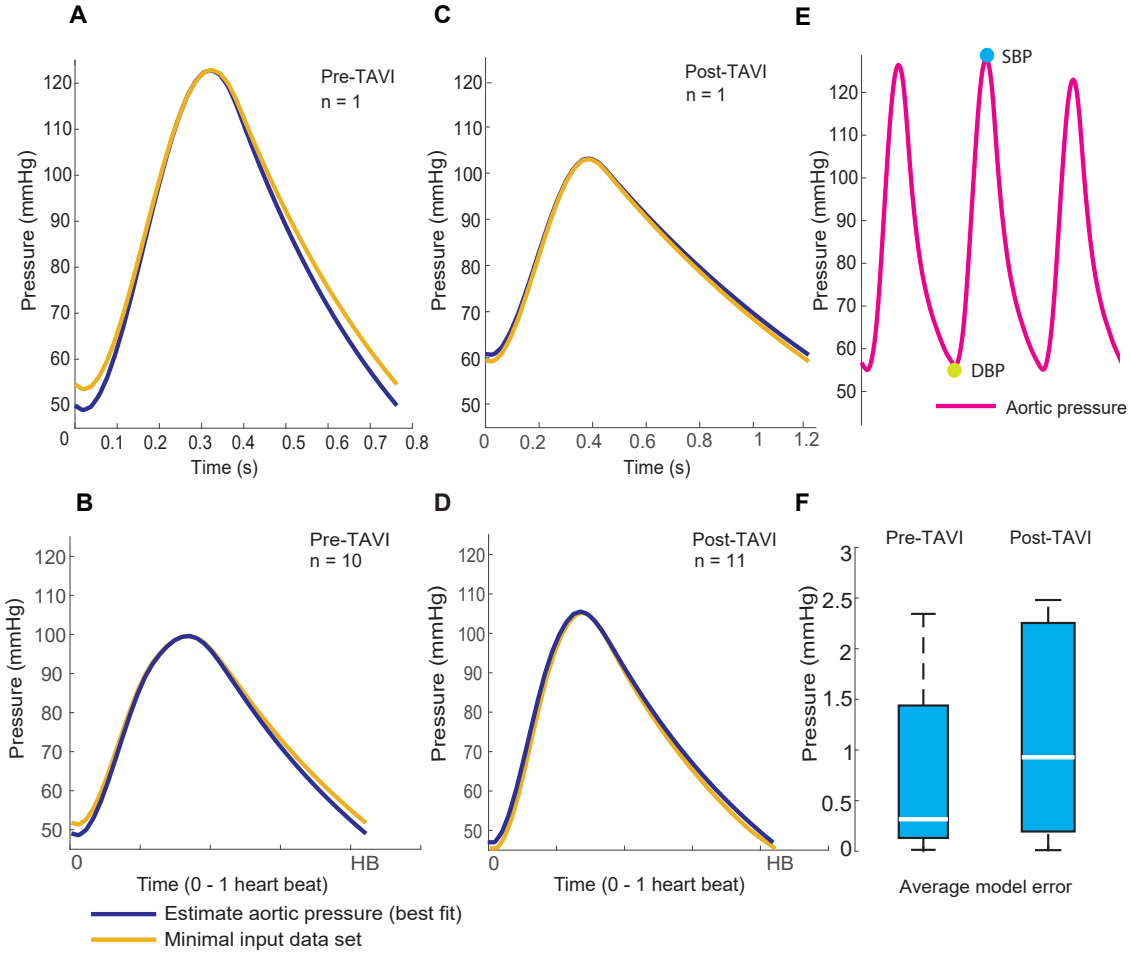

Figure 3. Aortic pressure can be estimated with a noninvasive minimal data set including DBP & SBP

A & C An example from one patient of aortic pressure estimated with the noninvasive minimal data set, pre-TAVI (**A**) and post-TAVI (**C**). This estimate (yellow) is compared to the output of the 3EWK model (dark blue) when it is optimally fit to the invasively measured pressure data. **B & D** The performance of the 3EWK using the minimal data set compared to the optimal fit is summarized for all patients. The mean average pressure estimate using DBP and SBP is shown in yellow, and the optimal fit is shown in dark blue. **F** Pre-TAVI, the average model error is 1.5 mmHg, post-TAVI, the error is 4.1 mmHg. E the timing of DBP and SBP in the pressure curve is shown.

widely described in literature. A sum of the sample patients' known parameters, weighted by their similarity to the new patient, was then used to estimate the aortic pressure curve. In figure 4 we see that this method estimated the aortic pressure curve with relatively poor accuracy. Since the sample sizes used in this study are low for machine learning standards, this is to be expected. Strikingly, though, we see that the stricter the algorithm becomes in determining probable vascular similarity, the lower the error becomes (figure 4, panel D & F). This decrease in model error is only valid until the inclusion radius becomes so small that very few (here, one or two) patients are included in the weighted average, resulting in an unreliable prediction. This indicates the merit of this technique, but also confirms the need for larger training groups.

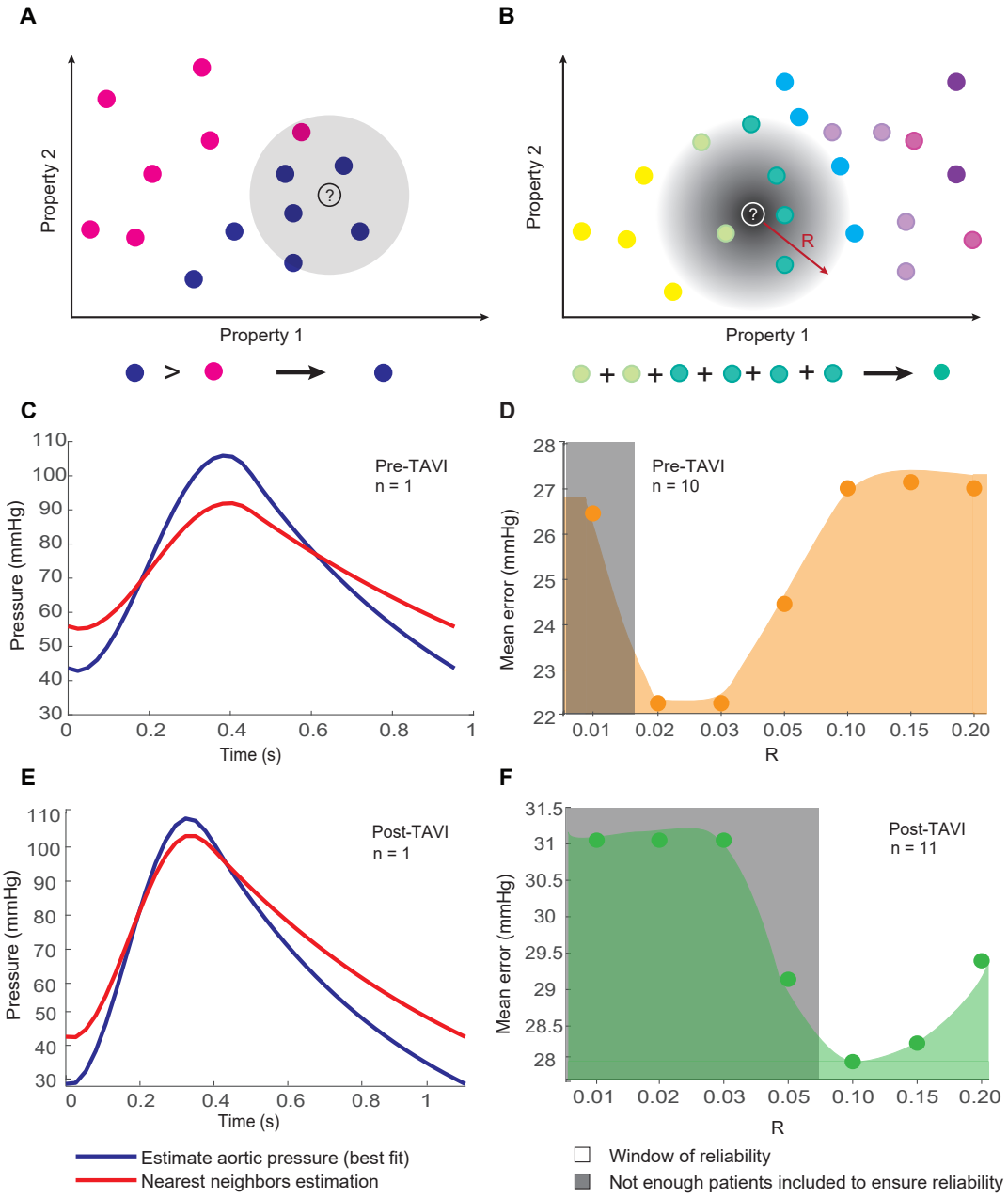

Figure 4. Nearest-neighbors inspired parameter estimation technique

A An illustration of a simple form of nearest neighbors classification. The question mark denotes an unclassified data point. The grey circle indicates the radius within which neighboring data points are taken into account for the unknown data point's classification. Within this circle, the majority of the data points are dark blue, so the question mark will also be labeled dark blue. **B** An illustration of the implemented parameter estimation technique which is inspired by nearest neighbors classification. Here, the data points represent the patients of which the optimal model parameters have been estimated by fitting the model to invasively measured pressure data. Each patient is given a location in a space spanned by their properties (age, BMI, gender). To estimate a new patient's model parameters, the patients within radius R from them are taken into account. A weighted average of their parameter values, where the weights are determined by the Euclidean distance to the patient in question, is used to find an estimate of the new patient's model parameters. **C & D** An example of the output of the 3EWK with nearest-neighbors estimated parameter values, with inclusion radius R = 0.05. Both examples perform poorly, which is to be expected because of the low sample group size. However, we see that the average output error becomes lower when the inclusion radius becomes smaller (**E & F**). This indicates that - up to a certain point - the technique becomes more reliable when the measure of similarity becomes stricter. When R becomes too small, too few patients are included in the average, resulting in a loss of performance.

Chapter 4

Discussion

We have developed and tested a new cardiac evaluation method that is noninvasive, fast, and can be applied in many settings, such as the ICU, the OR, and from the bedside. For this purpose, a model of the circulatory system was developed that can be used to accurately estimate LV pressure and volume, so as to allow LV PV loop reconstruction with exclusively noninvasive inputs extracted from ultrasound images. Ultrasound - which can be used in many settings, including at the bedside - allows for real-time noninvasive imaging of the LV. In combination with TOMTEC Arena cardiac quantification software, the LV volume can be retrieved from these images and used as an input for the aforementioned circulatory model, which in turn outputs an estimate of aortic pressure. We have shown that this method is successful, enabling cardiac function evaluation to be faster and more widely implementable, improving heart disease diagnosis and monitoring, which in turn improves overall prognosis. We saw that the aortic pressure curve could be reconstructed using only DBP and SBP as data points to fit the parameters of our model to, showing promise as a noninvasive parameter estimation method (mean error = 0.80 mmHg pre-TAVI and 1.6 mmHg post-TAVI, with respective Spearman correlations 0.9996 and 0.9950). Furthermore, we saw that machine learning techniques based on the correlation between patient information (age, BMI, gender) and vascular properties (compliance, resistance, impedance) can be implemented as an alternative noninvasive parameter estimation method, but more data is necessary to further develop and validate this technique.

Improvements in diagnosis and monitoring of heart disease are necessary - especially taking into account that we are currently living in an aging society, where heart disease will only become more common as life expectancy rises [69, 50, 28]. Besides offering a solution to the obvious health risks associated with an increased need for heart disease detection, a fast, cheap, and noninvasive cardiac evaluation system could also play a big role in preventing socioeconomic consequences of a rise in the prevalence of heart disease. Socioeconomic status has been shown to be an accurate predictor of cardiac health[17, 23, 58], as a result of biological, behavioral, and psychosocial characteristics of population groups with different levels of income, education, and access to healthcare, in developed societies[58, 17]. Even more, since clinical treatment of heart disease is expensive and prolonged, it can be a larger financial burden on population groups with a lower socioeconomic status. Because heart disease often occurs in middle aged people who are in a prime wage earning phase of life, this leaves families without unmissable income, when patients become temporarily or permanently unfit for employment. If a cheaper - and therefore more accessible - technique became the state-of-the-art cardiac assessment method, this disparity could be considerably minimized through early diagnosis and prevention.

LV PV loops - which are informative of contractility, LV size, ventricular-arterial interaction, chamber stiffness, stroke work, and more - are clinically applied to diagnose valvular diseases, such as aortic or mitral stenosis and regurgitation[21, 41]. Other heart diseases that can be diagnosed with LV PV loops include dilated and restrictive cardiomyopathy [68, 70], which would typically require catheterization. However, the applications for a noninvasive cardiac evaluation method are not limited to diseases that mostly occur in elderly patients. By eliminating the need for catheterization to estimate aortic blood pressure, we have created a diagnosis and monitoring method that is suitable for patients who are too fragile for invasive blood pressure measurements, such as infants. For example, catheterization is conventionally used to diagnose and post-operatively monitor congenital heart disease, while an accurate, noninvasive diagnosis method could result in shorter hospital stays and reduced mortality [37]. The cardiac evaluation method we propose could even open up the possibility of diagnosing congenital heart disease in fetuses, as the feasibility of automatic segmentation of the fetal heart from ultrasound images has been shown previously [3, 8]. Furthermore, this method is suitable to be included in routine medical controls, so could also be useful in detecting heart diseases such as childhood aortic stenosis, which is currently often only discovered coincidentally after treatment of other cardiac comorbidities [49].

Another benefit to the cardiac evaluation method we describe here, is its speed. Reconstructing LV PV loops with ultrasound can be done in real-time, and could therefore improve the diagnosis of cardiac diseases where timing is critical. For example, type I and II aortic dissection are typically diagnosed with TEE, computed tomography (CT), and a magnetic resonance angiography, but would benefit from a faster diagnosis method[16]. Our method could be implemented to measure any significant discrepancy between aortic pressure and blood pressure in more distal arteries (measured by for example a Finapres or ClearSight), which could indicate dissection. Especially post aortic replacement surgery, noninvasive aortic pressure monitoring is important[16]. Since the method involves no radiation, long term exposure is a possibility.

Unfortunately, the ultrasound systems used to image with TEE and TTE are cumbersome and require a physician to operate them, which means they are suboptimal for long term continuous monitoring. For diagnosis purposes, patients can, for example, be advised to wear a Holter monitor for 24 hours or more, to observe what changes in the ECG during physical activity, sleep, and other behaviors. These patients need to go about their day-to-day life, which is not possible with TEE and TTE. However, ultrasound has been previously successfully designed into light-weight, wearable electronics. A wearable ultrasound patch has been developed, that can measure central blood pressure from proximal arteries, such as the carotid[71]. Its design can withstand stretch (up to 60% strains [71]), showing that wearable ultrasound patches are reliable during motion. This indicates that ultrasound could also be used to monitor LV PV loops during cardiac stress tests. The use of a wireless ultrasound based cardiac evaluation method for continuous monitoring instead of a Holter monitor, provides more information on cardiac health and also involves less behavioral limitations for patients that are being monitored. Still, designing an ultrasound patch for the purpose of imaging the left ventricle would require efforts in developing an adequate power source, as the patch would involve a much larger array of transducers than a patch measuring more superficial arterial blood pressure, requiring more energy for its operations. Other concerns relate to secure wireless communication between the patch and an external receiver.

While such a novel cardiac evaluation model seems promising, there are some potential limitations that should be kept in mind. First of all, 3D TEE - which was used to image the LV - has a low acquisition rate. This low timing resolution results in some features of the LV volume curve being lost. Despite our efforts to counteract this (as described in the methods, section *model development and personalization*), it can cause problems in the alignment with other signals, such as the pressure data. Secondly, TEE produces images are relatively noisy in comparison to, for example, TTE. This could introduce an error in the LV volume measurements that function as input for the circulatory model. If it were the case that the error which is introduced into the model as a result of the use of TEE was constant, then the expected noise could be quantified and accounted for. However, the quality of ultrasound images varies considerably from patient to patient (supp. figure 2) as a result of differences in anatomy. This can cause the accuracy and reproducibility of the measurement of LV volume - and subsequently the aortic flow rate that is calculated from this - to vary greatly between patients.

Besides variable patient anatomy, the operator of the TEE probe and the data analyst who determines whether the semi-automatically detected boundaries in the cardiac quantification are correct, both introduce additional variability into the data. This unpredictable quality makes it difficult to account for some constant, expected error in the measurement. On the contrary, a wearable ultrasound patch would not be prone to variations in noise caused by the probe operator. Furthermore, making use of software that completely automatically extracts LV volume from 3D ultrasound images, would eliminate the variable error introduced by data analysts performing semi-manual segmentation. At the moment, TTE is more compatible with automatic cardiac quantification software, while TEE requires some manual boundary adjustment. Clinical use of TEE as input for our model is unlikely, as it typically requires patients to be generally anesthetized, so use of TTE is more practical. If a wearable ultrasound patch could produce images of a similar quality as TTE, this could possibly also be compatible with automatic quantification software.

In any case, a constant imaging method must be chosen. Particularly, parameter estimation relies on the consistent use of one imaging method, be it TEE, TTE, or a wearable ultrasound patch. Especially parameter estimation using machine learning requires the collection of a training data base where the data was acquired with one imaging method, otherwise the parameter values cannot be translated to other patients, due to the differences in image noise. Even though reconstructing the aortic pressure curve using only a minimized data set consisting of DBP and SBP to fit the curve to, seems like a promising method, this requires noninvasive estimation of DBP and SBP. Estimation methods for this purpose exist, but their reliability is questionable [79, 67, 72]. Therefore, a completely noninvasive parameter estimation method such as the machine learning technique we described would be preferable, stressing the need for a consistent imaging technique. Another limitation to using machine learning for parameter estimation is the homogeneity of the training data base that we used. These data are exclusively measured from TAVI patients, who typically are elderly and unhealthy[54, 48]. For a nearest neighbors inspired technique to work, the training data base should consist of a more diverse group of patients.

Despite these issues, a model allowing the reconstruction of LV PV loop is a promising solution to the shortcomings of current cardiac assessment techniques. It allows for noninvasive and fast diagnosis and continuous monitoring of heart disease in all

settings, including the bedside of critical care patients. This means that it could substantially change heart disease treatment protocols, which is necessary in a world with an aging population.

Chapter 5

Supplementary figures

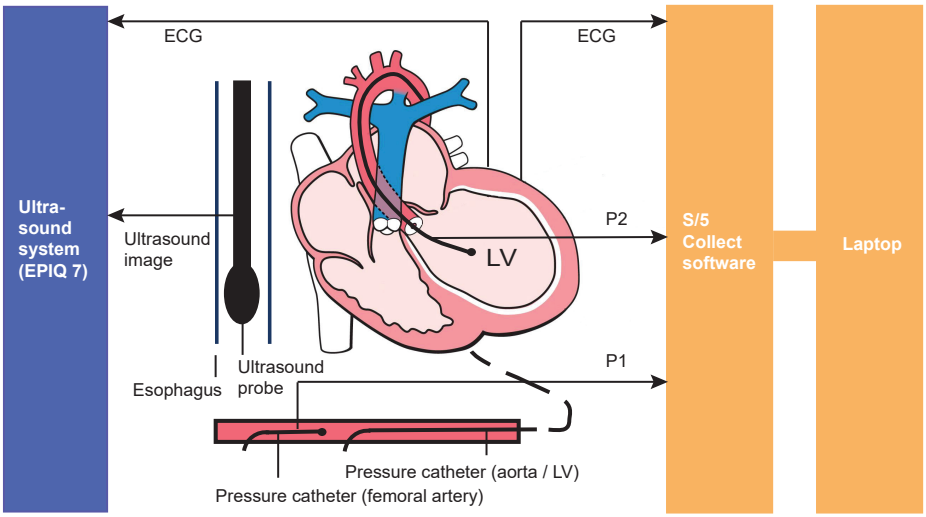

Supplementary figure 1. Data acquisition setup
The signals that are measured are collected in two different locations. Signals that are continuously collected (P1, P2, ECG) are stored on a drive through S/5 Collect software. During ultrasound imaging, a separate ECG signal is measured and saved inside the ultrasound image, which is stored on the EPIQ 7 ultrasound system. (Figure adapted from [1]).

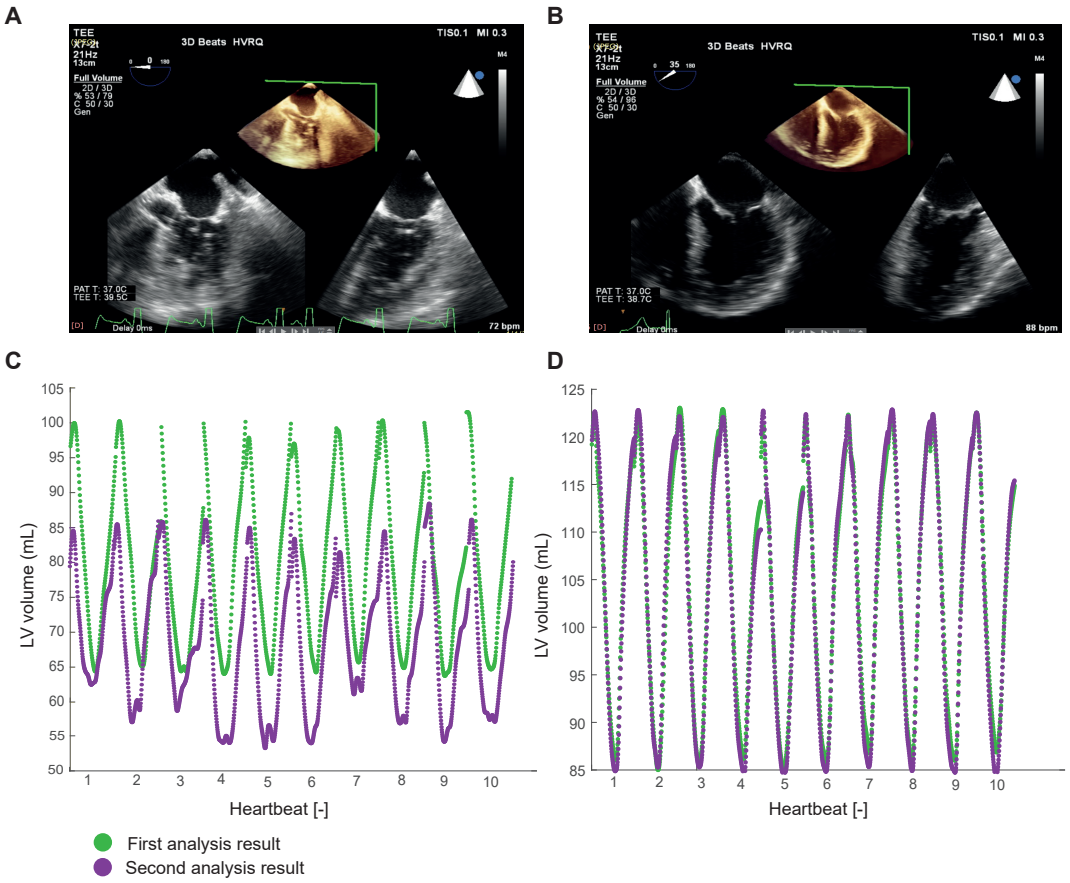

Supplementary figure 2. Reproducibility of noisy TEE-derived cardiac quantification
The noise level in TEE images largely depends on patient physiology, causing image quality to vary significantly. **A** An example of a noisy TEE image. **B** An example of a clear TEE image. **C & D** We see that the reproducibility of the noisy image (**A**) is low (**C**), whereas the reproducibility of the clear image (**B**) is high (**D**).

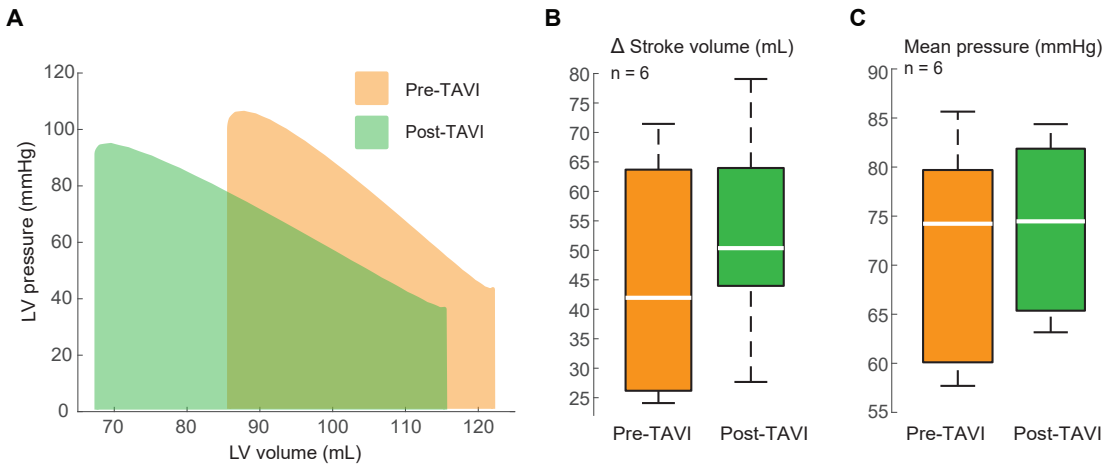

Supplementary figure 3. Comparison of left ventricular pressure-volume loops pre- and post-TAVI

A The pre- and post-TAVI PV loops of one patient show us that the TAVI procedure results in a larger stroke volume, as is expected. However, there is little change in pressure. **B** Boxplots summarizing the change in stroke volume and mean pressure for all patients (of which there was pre- and post-TAVI data available).

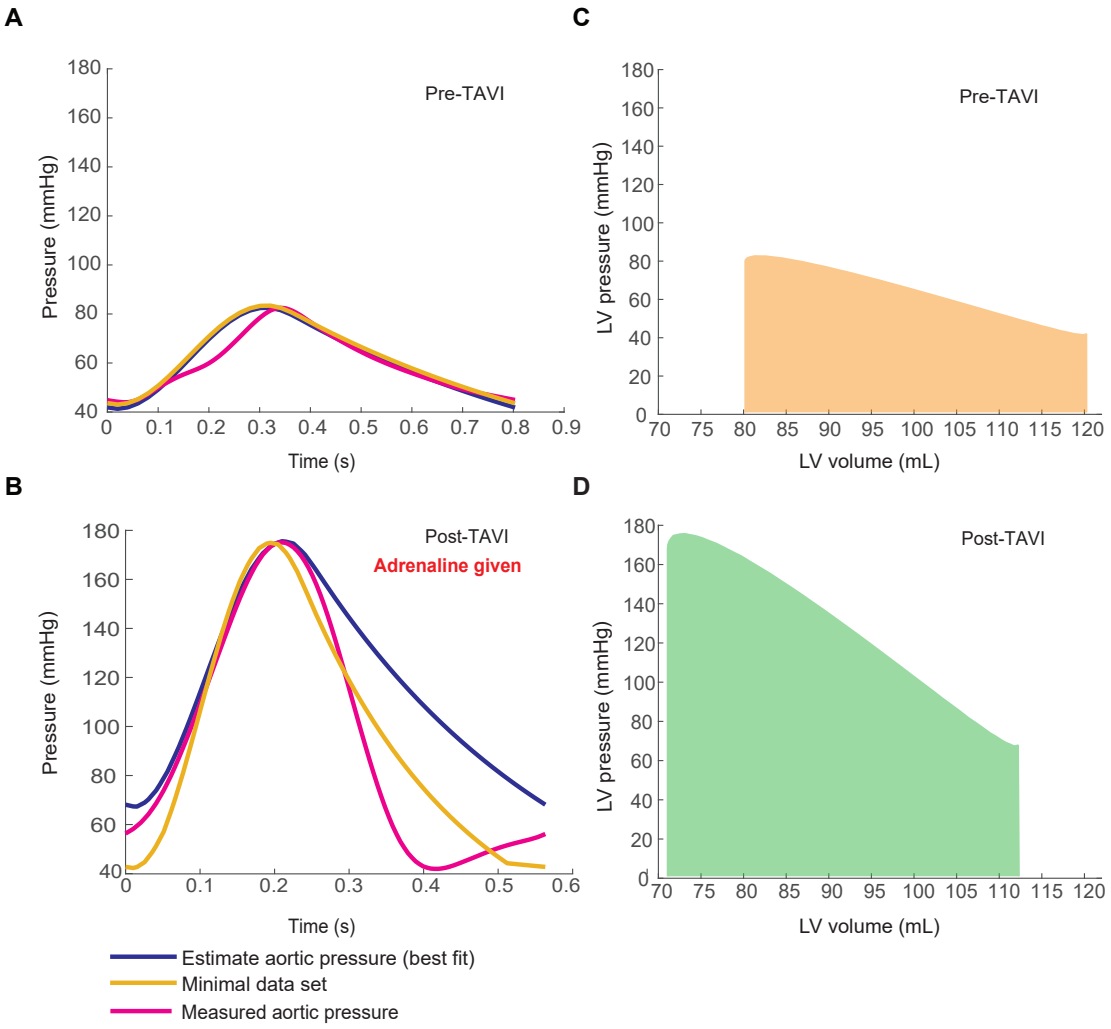

Supplementary figure 4. Case study showing the adaptability of the 3EWK model: Patient given adrenaline post-TAVI

A & B Aortic pressure (fuchsia) is reliably estimated by the optimally fit 3EWK model (dark blue), but also with only DBP & SBP (yellow). Even when adrenaline is given and the circulatory system takes on unnatural characteristics (**B**), the afore-mentioned estimation methods are reasonably reliable. **C & D** The PV loops reconstructed with aortic pressure estimated with the optimally fit 3EWK model.

Appendix A

Optimal measures for cardiac evaluation

A.0.1 Conventional (invasive) measurements for peri-operative cardiac monitoring

Since William Harvey's discovery of the circulation of blood through the vascular system in 1628, hemodynamics have been a vast information source of patients' cardiac health. However, difficulty with the availability of pressure and flow measurements presented this field with great challenges. Several methods, such as cardiac catheterization, have been developed since then, giving us access to these measurements and opening up a new opportunity to quantify cardiac properties and monitor changes in cardiac health. As these techniques are invasive, they are met with quite some challenges in regards to clinical implementation. Other attempts have recently been made which present noninvasive ways of measuring cardiac parameters[13, 36, 6], which could be useful in developing a more noninvasive cardiac evaluation set-up. Still, in both invasive and noninvasive methods, there is some consensus on which cardiac parameters are most informative of cardiac function.

Measures of cardiac function

Stroke volume and cardiac output First of all, stroke volume (SV) is used as a measure of cardiac health, providing information about preload, afterload, and contractility. It is defined as the amount of blood that is ejected by the heart in one heartbeat:

$$SV\ [mL] = ESV\ [mL] - EDV\ [mL] \tag{A.1}$$

Where:

$ESV\ [mL]$: is the end-systolic volume.
$EDV\ [mL]$: is the end-diastolic volume.

In diseased hearts, SV is sensitive to changes in afterload, which is not the case for healthy hearts.
Cardiac output (CO) is the total blood volume ejected by the left ventricle in a specific period of time:

$$CO\ [mL/S] = SV\ [mL] \cdot HR\ [1/S] \tag{A.2}$$

Where:

$HR\ [1/S]$: is the heart rate.

CO portrays similar information as SV, but is more often used as a measure of how well nutrients are transported throughout the body.

Ejection fraction Next, ejection fraction (EF) is widely used as an indicator of cardiac contractility. However, as it is quantified as the portion of the end diastolic volume that leaves the left ventricle after each contraction, EF is sensitive to afterload and heart size. This makes it an unreliable indicator of contractility, but rather, it offers more of an integrated measure of contractility, ventricular-arterial coupling, and ventricle size[7, 38].

$$EF\ [-] = EDV\ [mL]/SV\ [mL] \tag{A.3}$$

dP/dt$_{max}$ Furthermore, the maximal rate of pressure change during isovolumic contraction (dP/dt$_{max}$) is also used as a measure of contractility. However, it is sensitive to cardiac filling, and can underestimate contractility when heart rate rises, making it a sub-optimal measure.

Pressure-volume (PV) loops Where EF and dP/dt$_{max}$ have shortcomings due to their sensitivity to preload, afterload, heart rate, and remodeling, there are quantities independent from these factors that can be derived from the relationship between left ventricular pressure and volume. Pressure-volume loops can be constructed from this interaction, and from their shape we can compute the end systolic pressure-volume relationship (ESPVR) and the end diastolic pressure-volume relationship (EDPVR). As we see in figure A.1, the ESPVR is established by connecting the end-systolic points, whereas EDPVR is its diastolic analogue. ESPVR gives a meaningful indication of contractile function. On the other hand, EDPVR is the most important indicator of passive ventricular properties, as information from the diastolic phase gives us a clear idea of the preload that results from specific LV pressures, telling us a lot about chamber geometry. Therefore, both ESPVR and EDPVR are important measures to be considered peri-operatively when assessing ventricular function.

While the EDPVR is nonlinear, the ESPVR is fairly linear and can be characterized by its slope - the left ventricular end-systolic elastance (E$_{es}$, see figure A.2), described by:

$$E_{es}\ [mmHg/mL] = ESP\ [mmHg]/(ESV\ [mL] - V_0\ [mL]) \tag{A.4}$$

E_{es} gives a measure of the chamber stiffness at the end of systole, which provides information on the sensitivity of systolic pressure to vascular loading [32].

Besides ESPVR, EDVPR, and E$_{es}$, arterial elastance (E$_a$) has been considered of importance in characterizing ventricular-arterial interaction (figure A.2). E$_a$ is the negative slope if the line between the end-systolic pressure (ESP) and the end-diastolic volume (EDV), quantified as:

$$E_a\ [mmHg/mL] = ESP\ [mmHg]/SV\ [mL] \tag{A.5}$$

Ventricular-arterial coupling is then shown by the ratio E$_a$/E$_{es}$, which has been seen to be associated with prognosis in chronic heart failure[38]:

$$E_a/E_{es}\ [-] = \frac{ESV - V_0}{SV} \tag{A.6}$$

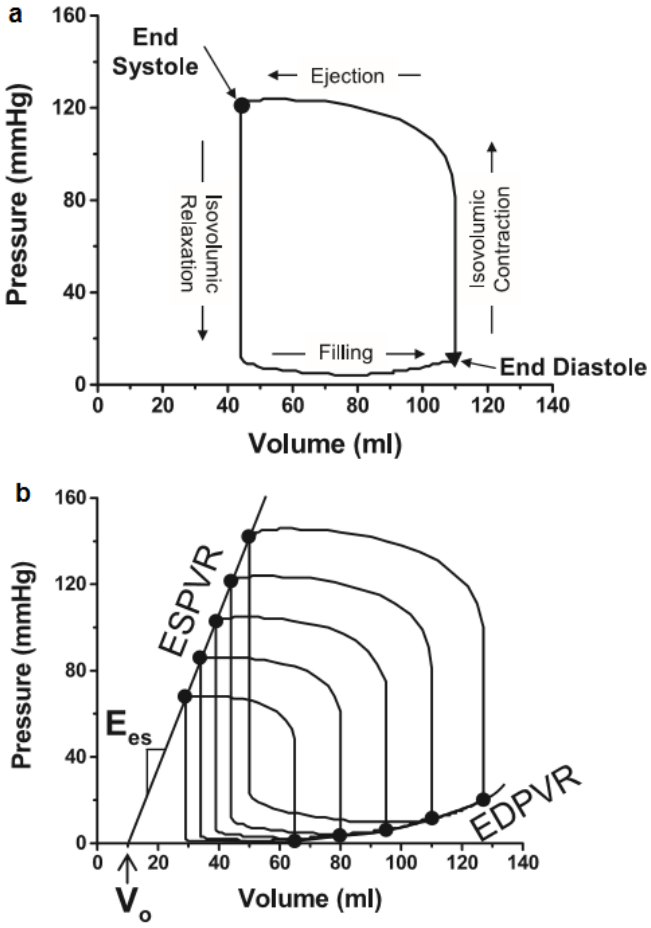

FIGURE A.1: Pressure-volume loops [10]

E_{es}, E_a, ESPVR, EDPVR, and other parameters that can be obtained from PV loops have been established to be meaningful indicators of left ventricular performance and intrinsic properties[55, 56, 65, 66]. For example, LV size (V_0), which is a reliable indicator of prognosis in heart failure, can be extracted from the PV loop by finding the intercept of the ESPVR with the x-axis where LV pressure is 0 $mmHg$[38]. Also, the mechanical work done by the left ventricle, composed of stroke work and elastic potential energy, can be inferred from the area covered by the PV loop (figure A.3). However, obtaining both ESPVR and EDPVR involves varying cardiac load, which is highly invasive.

Some methods have been proposed for estimating ESPVR and E_{es} without loading interventions[61, 13, 62, 36]. These so-called single-beat estimation methods consider the relationship between LV pressure, volume, and elastance, making use of the left ventricle's elastic structure that shows predictable patterns in stiffening and relaxation throughout a cardiac cycle. Similar to what we see in equation A.4 and A.5, elastance can be seen as the ratio between left ventricular pressure and volume, and can be tracked over time. The time-varying elastance variable ($E(t)$) is defined as the following transformation between pressure and volume[66, 56, 61, 13]:

$$P(t) = E(t) \cdot [V(t) - V_0] \tag{A.7}$$

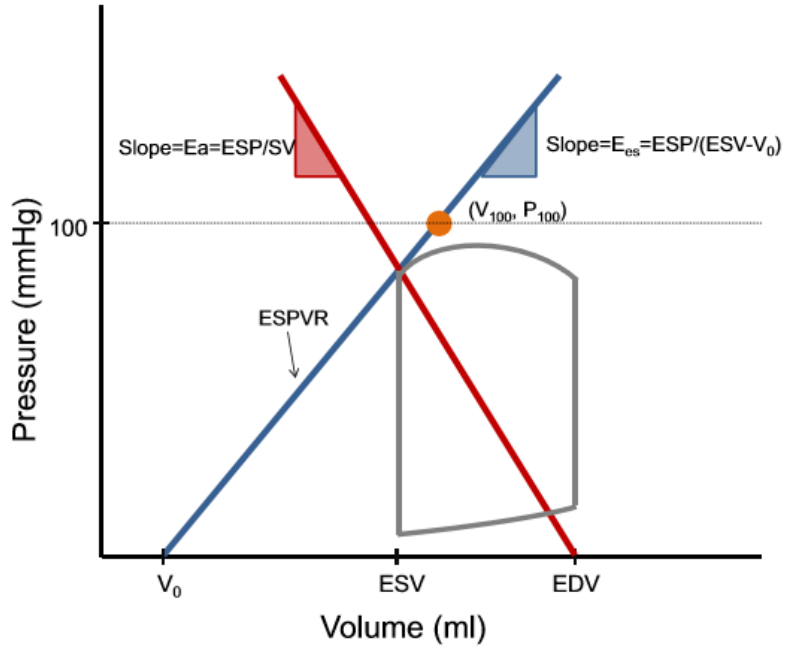

FIGURE A.2: PV loop showing aterial elastance E_a [38]

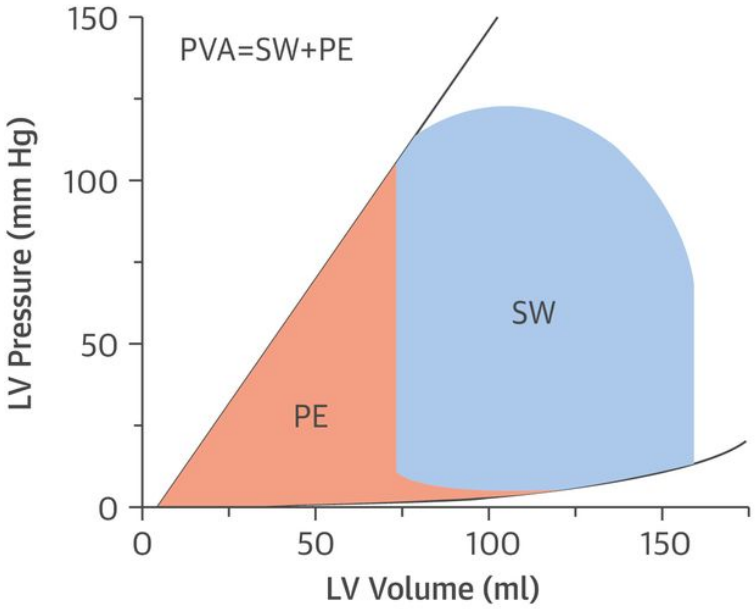

FIGURE A.3: Mechanical work done by left ventricle [12].

When normalized by maximum amplitude and time to peak amplitude, the elastance curve has a typical waveform (figure A.4). The normalized elastance curve is consistent regardless of contractile state, heart rate, and cardiac loading conditions, such as end-diastolic volume or aortic pressure[65, 66]. Furthermore, it upholds for patients with different types of myocardial disease[61]. The consistency of this waveform has been questioned by studies that say the linear behavior of the ESPVR does not hold up for extreme LV loading conditions[33, 11, 5, 9]. However, such loading conditions are unlikely to occur in live human patients, as the loading conditions are constrained here. Therefore we can still assume load-independence of the

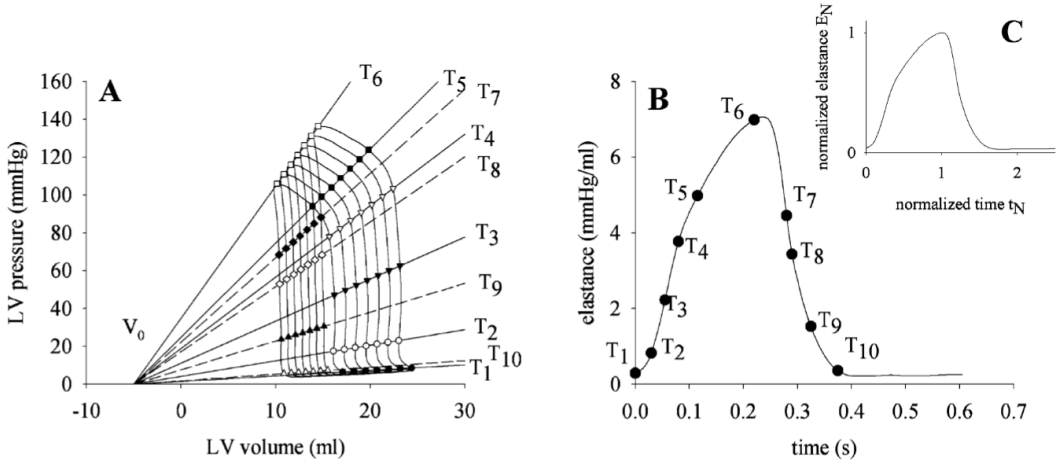

FIGURE A.4: Normalization of time-varying elastance waveform [59]

elastance curve[61].

Single-beat methods provide a reliable way of avoiding needing loading-interventions in order to find ESPVR and EDPVR. However, constructing PV loops still requires invasive methods, as LV pressure and volume must be measured through catheterization. Some attempts to reconstruct PV loops with exclusively noninvasive measurements have been made[13, 62, 36]. These estimation methods only require various combinations of arm-cuff arterial pressures, echo-Doppler cardiography, electrocardiography, sphygmometry, and radionucleotide ventriculography.
A similar non-invasive single-beat approach has been presented for estimation of the EDPVR[36], making use of Doppler-echocardiography, radionuclide ventriculography, and magnetic resonance imaging.

We conclude that PV loops provide meaningful indicators of cardiac health and passive properties of the left ventricle. Contrary to other common cardiac performance indicators, PV loops are not sensitive to preload, afterload, heart rate, or remodeling. Furthermore, they can clearly indicate many cardiac diseases, such as dilated or restrictive cardiomyopathy, left ventricular hypertrophy, and valvular diseases, such as stenosis or regurgitation. However, if PV loops are to be implemented in diagnosis and monitoring of heart disease, a method must be developed with which PV loops can be reconstructed noninvasively.

Appendix B

Derivation of governing equations for Windkessel models

B.1 Three-element Windkessel

The electric circuit analog of the three-element Windkessel is shown in figure B.1

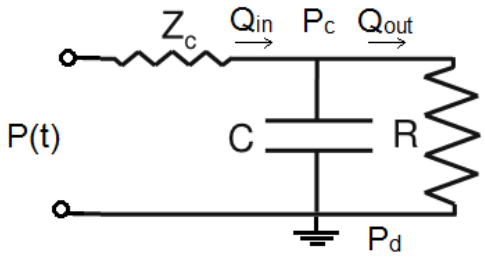

FIGURE B.1: Three-element Windkessel model electric circuit analog

The definition of capacitance is:

$$C = \frac{dV(t)}{dP_c(t)} \tag{B.1}$$

$$\frac{dP_c(t)}{dt} = \frac{dV(t)}{C} \tag{B.2}$$

$$\frac{dP_c(t)}{dt} = \frac{1}{C}\frac{dV(t)}{dt} \tag{B.3}$$

$$C\frac{dP_c(t)}{dt} = Q_{in}(t) - Q_{out}(t) \tag{B.4}$$

As a result of the circuit topology, we define Q_{in} and Q_{out} as:

$$Q_{in}(t) = \frac{P(t) - P_c(t)}{Z_c} \quad \text{and} \quad Q_{out}(t) = \frac{P_c(t) - P_d(t)}{R} \tag{B.5}$$

Then if follows that:

$$C\frac{dP_c(t)}{dt} = \frac{P(t) - P_c(t)}{Z_c} - \frac{P_c(t) - P_d(t)}{R} \tag{B.6}$$

Since $P_d(t) = 0$:

$$C\frac{dP_c(t)}{dt} = \frac{P(t) - P_c(t)}{Z_c} - \frac{P_c(t)}{R} \tag{B.7}$$

From the circuit topology we know that:

$$P_c(t) = P(t) - Z_c Q_{in}(t) \tag{B.8}$$

If we combine equations B.7 and B.8:

$$C\frac{d}{dt}(P(t) - Z_c Q_{in}(t)) = \frac{P(t) - (P(t) - Z_c Q_{in}(t))}{Z_c} - \frac{P(t) - Z_c Q_{in}(t)}{R} \tag{B.9}$$

$$C\frac{dP(t)}{dt} - CZ_c\frac{dQ_{in}(t)}{dt} = \frac{P(t)}{Z_c} - \frac{P(t)}{Z_c} + \frac{Z_c Q_{in}}{Z_c} - \frac{P(t)}{R} + \frac{Z_c Q_{in}(t)}{R} \tag{B.10}$$

$$C\frac{dP(t)}{dt} + \frac{P(t)}{R} = (1 + \frac{Z_c}{R})\frac{dQ_{in}(t)}{dt} \tag{B.11}$$

B.2 Four-element Windkessel

The electric circuit analog of the four-element Windkessel model is shown in figure B.2

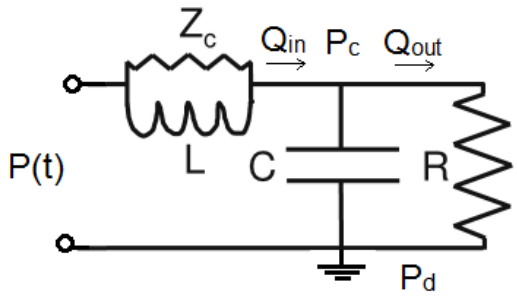

FIGURE B.2: Four-element Windkessel model electric circuit analog

If we start with the definition of the rate of pressure change in time given in equation B.4, and - given the circuit topology - we define Q_{in} and Q_{out} as:

$$Q_{in}(t) = \frac{P(t) - P_c(t) - L\frac{dQ_{in}(t)}{dt}}{Z_c} \quad \text{and} \quad Q_{out} = \frac{P_c}{R} \tag{B.12}$$

Then we can combine equations B.4 and B.12:

$$C\frac{dP_c(t)}{dt} = \frac{P(t) - P_c(t) - L\frac{dQ_{in}(t)}{dt}}{Z_c} - \frac{P_c}{R} \tag{B.13}$$

It follows from the circuit topology that we can express $P_c(t)$ in terms of $P(t)$ as:

$$P_c(t) = P(t) - Z_c Q_{in}(t) - L\frac{dQ_{in}(t)}{dt} \tag{B.14}$$

Then we can combine equations B.13 and B.14:

$$C\frac{d}{dt}(P(t) - Z_c Q_{in}(t) - L\frac{dQ_{in}(t)}{dt}) = \frac{P(t) - (P(t) - Z_c Q_{in}(t) - L\frac{dQ_{in}(t)}{dt}) - L\frac{dQ_{in}(t)}{dt}}{Z} - \frac{P(t) - Z_c Q_{in}(t) - L\frac{dQ_{in}(t)}{dt}}{R} \tag{B.15}$$

$$C\frac{dP(t)}{dt} + \frac{P(t)}{R} = (1 + \frac{Z_c}{R})Q_{in}(t) + (\frac{L}{R} + \frac{C}{Z_c})\frac{dQ_{in}(t)}{dt} + CL\frac{d^2Q_{in}(t)}{dt^2} \tag{B.16}$$

Appendix C

Model development

Model development

A model is a simplified representation of reality, that provides an opportunity to study a process ex vivo, without ethical constraints, in order to gain a better understanding of its workings. Studying the circulatory system noninvasively requires a model, as some values cannot be obtained, but must be predicted. Numerous types of models describing the cardiovascular system have been developed, ranging from lumped parameter models or zero-dimensional (0D) models suitable for modelling circulation, one-dimensional (1D) models that are appropriate for simulating blood pressure and flow, to three-dimensional (3D) models capable of modelling interaction of fluid with cardiovascular structures, such as cardiac diseases.

In this work, our aim is to model measures such as pressure, volume, and flows at the entrance of the vascular system (in the left ventricle and around the aortic valve), and not complex local changes of pressure and flow, nor interactions of fluids and cardiac structures. Lumped parameter models provide a pressure-flow relation that is sufficient for our needs. Therefore, we focus mainly on zero-dimensional lumped parameter models.

Lumped parameter (0D) models

Lumped parameter models decompose physiological systems into elementary physical components that follow established physical laws, so their relationships can be expressed by simple mathematical equations. As more knowledge was gained of the cardiovascular system, such mathematical descriptions of it became more accurate.

Anatomical components of the circulation system can be modelled by analog electric circuit elements, each element representing a different circulatory component. To this extent, the heart pumping blood throughout the systemic system is seen as a current source providing flow. Pressure differences are seen as voltages, and volume is seen as charge. The vasculature is then represented by lumped parameters; a resistor, which simulates the resistance to blood flow largely due to the capillaries; a capacitor, which represents the elasticity or compliance of the vessels; impedance, which models the afterload that the left ventricle must overcome during a contraction; and an inductor, which incorporates the inertance of the blood mass that is propelled by the pumping force of the heart. Modelling the circulatory system as an electric circuit gives us the opportunity to simulate blood pressure dynamics. The combination of electric components used depends on which type of model is implemented.

Two-element Windkessel model Historically, it was thought that peripheral resistance of the vascular system was the main determinant of blood pressure. However, Hales (1735) noticed that, during a heartbeat, arterial pressure varies due to changes in arterial compliance as a result of the elastic response of arteries to volume being pumped through by the left ventricle. When this became clear, arterial compliance was also acknowledged as an important contributor to blood pressure.
In the 1800s, the similarity between the large arteries and the Windkessel of a fire engine was proposed (figure C.1). Later on, in 1899, the first Windkessel model of the cardiovascular system was formulated[20], describing the pressure-flow relationship at the entrance of the vascular system. It includes the peripheral resistance and arterial compliance as the two main determinants of the system and is therefore named the two-element Windkessel model (figure C.2).

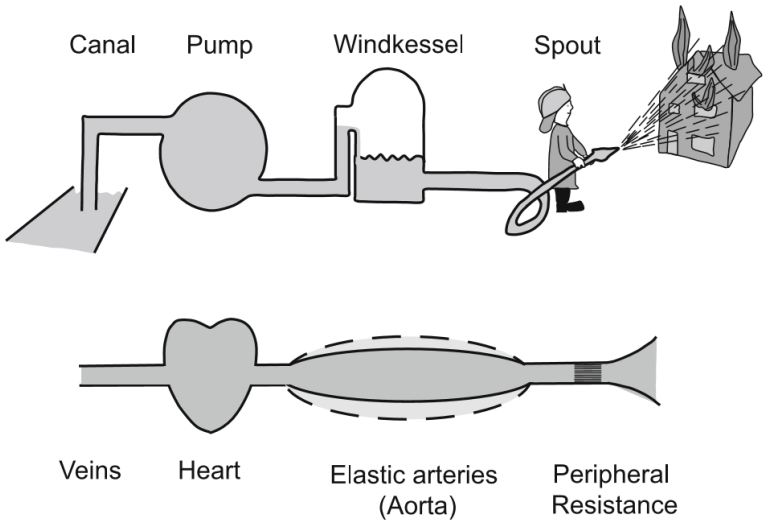

FIGURE C.1: Windkessel model of the circulation system [74]

The governing equations of the two-element Windkessel model are as follows[44]:

The continuity equation shows us that the inflow of blood into the aterial system at the aortic valve equals the outflow of blood from the aterial system into the venous system.

$$\frac{dV(t)}{dt} = Q_{in}(t) - Q_{out}(t) \tag{C.1}$$

Compliance of the aterial system is defined as the rate of volume change due to a pressure change:

$$C = \frac{dV(t)}{dP(t)} \tag{C.2}$$

The pressure drop over the resistance of the arterial system gives an indication of the blood flow into the venous system:

$$Q_{out}(t) = \frac{P(t)}{R} \tag{C.3}$$

Where resistance is given by R.
Combining equations C.1, C.2, and C.3, gives us:

$$C\frac{dP(t)}{dt} + \frac{P(t)}{R} = Q_{in}(t) \tag{C.4}$$

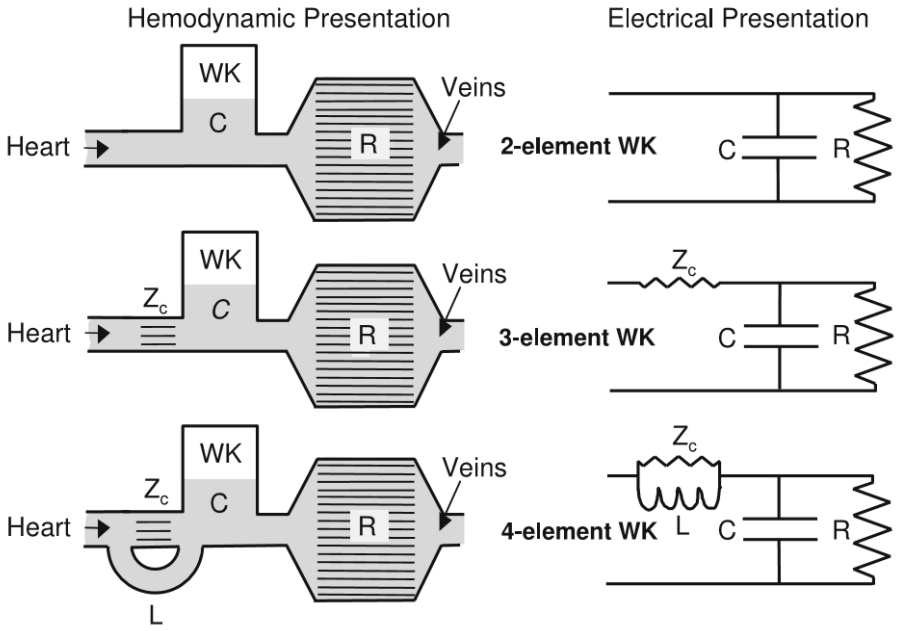

FIGURE C.2: Equivalent circuits of the circulation system [74]

Note that this is the case for systole, whereas during diastole, there is no flow into the arterial system. This means that Q_{in} is zero, so:

$$C\frac{dP(t)}{dt} + \frac{P(t)}{R} = 0 \tag{C.5}$$

Three-element Windkessel model Fourier analysis showing input impedance later revealed that the two-element Windkessel model poorly described the pressure-flow relation at high frequencies, as occur during systole[75]. At these frequencies, the modulus of the impedance approaches zero and its phase becomes -90°, while in reality, the modulus of the arterial system's input impedance approaches a plateau value and the phase becomes approximately zero[74]. To account for this effect at high frequencies, a third component was proposed in the three-element Windkessel model. Here, the characteristic impedance of the proximal aorta that models the afterload that the left ventricle must overcome, is added to the electric circuit analog (figure C.2), which equals the plateau value that was seen before at high frequencies:

$$Z = \frac{v\rho}{A} \tag{C.6}$$

Where:

- Z: is the characteristic impedance of the proximal aorta
- v: is the blood wave speed
- ρ: is the blood density
- A: is the cross-sectional area of the proximal aorta

In the frequency domain, the impedance of the complete three-element Windkessel simply is given by the addition of the two-element Windkessel input impedance with the characteristic impedance of the proximal aorta, as these are connected in

series:

$$Z_{input} = Z_c + \frac{R}{1 + j\omega RC} \tag{C.7}$$

In the time domain the governing equation (derivation shown in appendix B) then becomes:

$$\frac{P(t)}{R} + C\frac{dP(t)}{dt} = (1 + \frac{Z_c}{R})Q_{in}(t) + Z_c C\frac{dQ_{in}(t)}{dt} \tag{C.8}$$

Four-element Windkessel model As can be seen in figure C.2, the characteristic impedance of the proximal aorta is represented by a resistor. This is logical as they share the same dimensions. However, in reality it is not an actual resistor, which creates some problems in the lower frequencies, where the impedance is highest. In the three-element Windkessel model, total resistance becomes:

$$R_{total} = R_{peripheral} + Z \tag{C.9}$$

This leads to errors when the impedance is high. Fortunately, when compared to total peripheral resistance, the value of impedance of the proximal aorta is only approximately 5-7% of its size, so the errors are only small. Still, a fourth component has been proposed to correct for this.

An inductor can be added (figure C.2), which represents the total arterial inertance. As the characteristic impedance of the proximal aorta already takes the inertance of the proximal aorta into account, this addition largely affects the lower frequencies. The total arterial inertance is calculated by adding the inertances of all the arteries, but it is difficult to estimate its value. This is the main reason why three-element Windkessel models are often preferred over four-element Windkessels.

The input impedance in the frequency domain of the four-element Windkessel electric circuit analog where an inductor is added in parallel with the characteristic impendance of the proximal aorta (figure C.2) is then:

$$Z_{input} = \frac{j\omega LZ_c}{Z_c + j\omega L} + \frac{R}{1 + j\omega RC} \tag{C.10}$$

The time domain governing equation (derivation in appendix B) is given by:

$$C\frac{dP(t)}{dt} + \frac{P(t)}{R} = (1 + \frac{Z_c}{R})Q_{in}(t) + (\frac{L}{R} + CZ_c)\frac{dQ_{in}(t)}{dt} + CL\frac{d^2Q_{in}(t)}{dt^2} \tag{C.11}$$

Comparison of Windkessel models All types of Windkessel models have their merits and their faults. For example, the two-element Windkessel model has few parameters that must be estimated, which makes the required computations simpler. However, it performs poorly for high frequency input and does not describe distal pressures well, as wave propagation effects are not considered in this model. To this extent, it assumes that pressure rises simultaneously in the whole arterial system, even though this is not the case. Therefore, the pressure waveform prediction for distal arteries is inaccurate.

While the three-element Windkessel model does attempt to incorporate wave propagation effects, its biggest drawback is that it overestimates the total resistance, which causes poor performance at low frequencies.

The four-element Windkessel does account for this, and it shows the best fit to measured pressure waveforms. However, the inertance parameter L is difficult to

estimate, which is a drawback. Also, the complexity of the model means that its parameter estimation will require a lot of computation and time. Depending on the application of the model, long computation time might outweigh the benefits of a better performance. As this is the case in our application, a three-element Windkessel model will suffice.

	Two-element WK	Three-element WK	Four-element WK
P_{diast}	RC-time	RC-time	RC-time
Total waveshape	Poor	Good	Good
Impedance	Poor at high freq.	Small error at low freq.	Good at all freq.
Compliance	Good	Overestimation	Accurate
Inertance	NA	NA	Difficult
$P_{mean}/flow_{mean}$	Resistance	Resistance + charact. imp.	Resistance

TABLE C.1: Comparison of Windkessel models [74]

Appendix D

Approval Medical Ethics Committee

Michelangelolaan 2 - 5623 EJ Eindhoven
Postbus 1350 - 5602 ZA Eindhoven
www.catharinaziekenhuis.nl

catharina ziekenhuis

geadresseerde:
Dr. R.A. Bouwman, Anesthesioloog

ALHIER

afdeling: Medical research Ethics Committ United (MEC-U)
doorkiesnummers 040 – 239 8402
contactpersoon: 040 – 239 8716
Afdeling: 040 – 239 8716

onze referentie: M16-0049
kopie:

datum: Eindhoven, 29 februari 2016

betreft: **Niet-WMO Verklaring MEC-U**

Protocol: Perioperative ultrasound database
Registratienummer: **niet-WMO 2015-90**

Geachte heer Bouwman,

Betreffende bovengenoemde studie delen wij u mede dat MEC-U van mening is dat deze studie niet WMO-plichtig is, aangezien er geen sprake is van het onderwerpen van personen aan handelingen of het opleggen aan personen van een bepaalde gedragswijze.

De commissie heeft het onderzoeksprotocol alleen getoetst in het kader van de zorgvuldigheid ter verkrijging van een verklaring van geen bezwaar. Het toetsingskader voor het onderzoek is derhalve niet de WMO, maar de Gedragscode Gezondheidsonderzoek (Code goed gedrag, zie www.federa.org), alsmede de Wet bescherming persoonsgegevens (WBP). De Gedragscode Gezondheidsonderzoek vormt een uitwerking van met name het bepaalde in de Wet op de geneeskundige behandelingsovereenkomst (WGBO) over het gebruik van patiëntengegevens in wetenschappelijk onderzoek.

Mits u de Gedragscode Gezondheidsonderzoek alsmede de WBP in acht neemt, hebben wij geen bezwaar tegen uitvoeren van het onderzoek.

Met vriendelijke groet,

Mw. drs. M.S.E. van Poeijer, ambtelijk secretaris

Namens dr. R.J.E. Grouls
voorzitter Medical research Ethics Committees United (MEC-U)

Documenten:
- Aanbiedingsmail d.d. 23-12-2015
- Aanbiedingsbrief d.d. 15-12-2015 9Ontvangen d.d. 23-12-2015)
- Registratieformulier Niet-WMO onderzoek d.d. 15-12-2015
- Patiënteninformatie v1.0, d.d. oktober 2014

NW02

een santeon ziekenhuis

Bibliography

[1] Admin. "Hypoplastic Left Heart Syndrome and Critical Aortic Stenosis". In: *Obstetric, Gynecology and Pediatric Insight Engine* (2016).

[2] Koen Ameloot, Pieter-Jan Palmers, and Manu LNG Malbrain. "The accuracy of noninvasive cardiac output and pressure measurements with finger cuff: a concise review". In: *Current opinion in critical care* 21.3 (2015), pp. 232–239.

[3] Sansanee Auephanwiriyakul, Nipon Theera-Umpon, Theera Tongsong, et al. "Patch-based fetal heart chamber segmentation in ultrasound sequences using possibilistic clustering". In: *2015 Seventh International Conference on Computational Intelligence, Modelling and Simulation (CIMSim)*. IEEE. 2015, pp. 43–48.

[4] Alberto P Avolio et al. "Arterial flow, pulse pressure and pulse wave velocity in men and women at various ages". In: *Sex-Specific Analysis of Cardiovascular Function*. Springer, 2018, pp. 153–168.

[5] Jan Baan and Enno T Van Der Velde. "Sensitivity of left ventricular end-systolic pressure-volume relation to type of loading intervention in dogs." In: *Circulation research* 62.6 (1988), pp. 1247–1258.

[6] CA Boly et al. "Minimally invasive intraoperative estimation of left-ventricular end-systolic elastance with phenylephrine as loading intervention". In: *British journal of anaesthesia* 111.5 (2013), pp. 750–758.

[7] Barry A Borlaug and David A Kass. "Invasive hemodynamic assessment in heart failure". In: *Cardiology clinics* 29.2 (2011), pp. 269–280.

[8] Christopher P Bridge, Christos Ioannou, and J Alison Noble. "Automated annotation and quantitative description of ultrasound videos of the fetal heart". In: *Medical image analysis* 36 (2017), pp. 147–161.

[9] DANIEL Burkhoff, PIETER P De Tombe, and WILLIAM C Hunter. "Impact of ejection on magnitude and time course of ventricular pressure-generating capacity". In: *American Journal of Physiology-Heart and Circulatory Physiology* 265.3 (1993), H899–H909.

[10] Daniel Burkhoff, Israel Mirsky, and Hiroyuki Suga. "Assessment of systolic and diastolic ventricular properties via pressure-volume analysis: a guide for clinical, translational, and basic researchers". In: *American Journal of Physiology-Heart and Circulatory Physiology* 289.2 (2005), H501–H512.

[11] DANIEL Burkhoff et al. "Contractility-dependent curvilinearity of end-systolic pressure-volume relations". In: *American Journal of Physiology-Heart and Circulatory Physiology* 252.6 (1987), H1218–H1227.

[12] Daniel Burkhoff et al. "Hemodynamics of mechanical circulatory support". In: *Journal of the American College of Cardiology* 66.23 (2015), pp. 2663–2674.

[13] Chen-Huan Chen et al. "Noninvasive single-beat determination of left ventricular end-systolic elastance in humans". In: *Journal of the American College of Cardiology* 38.7 (2001), pp. 2028–2034.

[14] W Cheng et al. “Comparison of invasive and non-invasive blood pressure in critically ill patients”. In: *Zhonghua yi xue za zhi* 98.37 (2018), pp. 3005–3008.

[15] Hyemoon Chung et al. “Arterial stiffness, sex, and age difference on hypertensive response to supine bicycle exercise”. In: *The Journal of Clinical Hypertension* 19.12 (2017), pp. 1260–1268.

[16] E Stanley Crawford. “The diagnosis and management of aortic dissection”. In: *Jama* 264.19 (1990), pp. 2537–2541.

[17] Felipe Díaz-Toro, Hugo E Verdejo, and Pablo F Castro. “Socioeconomic inequalities in heart failure”. In: *Heart failure clinics* 11.4 (2015), pp. 507–513.

[18] Lauren E. Gibson et al. “Comparison of Invasive and Noninvasive Blood Pressure Measurements for Assessing Signal Complexity and Surgical Risk in Cardiac Surgical Patients”. In: *Anesthesia Analgesia* (Nov. 2018), p. 1. DOI: 10.1213/ANE.0000000000003894.

[19] S. E. Francis. “Continuous Estimation of Cardiac Output and Arterial Resistance from Arterial Blood Pressure using a Third-Order Windkessel Model”. MA thesis. Massachussetts Institute of Technology, 2007.

[20] O Frank. “Die Grundform des arteriellen Pulses [Basic shape of the arterial pulse], Zeitschriftfür Biologie, vol. 37”. In: (1899).

[21] Kiyotaka Fukamachi et al. “Changes in mitral annular and left ventricular dimensions and left ventricular pressure–volume relations after off-pump treatment of mitral regurgitation with the Coapsys device”. In: *European journal of cardio-thoracic surgery* 25.3 (2004), pp. 352–357.

[22] Marcus Granegger et al. “Noninvasive assessment of blood pressure in rotary blood pump recipients using a novel ultrasonic Doppler method”. In: *The International journal of artificial organs* 42.5 (2019), pp. 226–232.

[23] Nathaniel M Hawkins et al. “Heart failure and socioeconomic status: accumulating evidence of inequality”. In: *European journal of heart failure* 14.2 (2012), pp. 138–146.

[24] I.H.F. Herald. “Assessment of cardiopulmonary function by contrast-enhanced echocardiography”. PhD thesis. TU Eindhoven.

[25] Po Hu et al. “A hospital-based survey of patients with severe valvular heart disease in China”. In: *International journal of cardiology* 231 (2017), pp. 244–247.

[26] Kuan-Hua Huang et al. “A Highly Sensitive Pressure-Sensing Array for Blood Pressure Estimation Assisted by Machine-Learning Techniques”. In: *Sensors* 19.4 (2019), p. 848.

[27] Bernard Iung and Alec Vahanian. “Degenerative calcific aortic stenosis: a natural history”. In: *Heart* 98.Suppl 4 (2012), pp. iv7–iv13.

[28] Bernard Iung and Alec Vahanian. “Epidemiology of acquired valvular heart disease”. In: *Canadian Journal of Cardiology* 30.9 (2014), pp. 962–970.

[29] Ye Jin et al. “Evaluation of carotid artery stiffness in obese children using ultrasound radiofrequency data technology”. In: *Journal of Ultrasound in Medicine* 32.1 (2013), pp. 105–113.

[30] Gaurav Kapur et al. “Noninvasive Determination of Blood Pressure by Heart Sound Analysis Compared With Intra-Arterial Monitoring in Critically Ill Children-A Pilot Study of a Novel Approach.” In: *Pediatric critical care medicine: a journal of the Society of Critical Care Medicine and the World Federation of Pediatric Intensive and Critical Care Societies* (2019).

[31] David A Kass. "Age-related changes in venticular–arterial coupling: pathophysiologic implications". In: *Heart failure reviews* 7.1 (2002), pp. 51–62.

[32] David A Kass and W Lowell Maughan. "From'Emax'to pressure-volume relations: a broader view." In: *Circulation* 77.6 (1988), pp. 1203–1212.

[33] David A Kass et al. "Influence of contractile state on curvilinearity of in situ end-systolic pressure-volume relations." In: *Circulation* 79.1 (1989), pp. 167–178.

[34] Syed Ghufran Khalid et al. "Blood pressure estimation using photoplethysmography only: comparison between different machine learning approaches". In: *Journal of healthcare engineering* 2018 (2018).

[35] Joshua Kim et al. "Soft Wearable Pressure Sensors for Beat-to-Beat Blood Pressure Monitoring". In: *Advanced healthcare materials* (2019), p. 1900109.

[36] Stefan Klotz et al. "Single-beat estimation of end-diastolic pressure-volume relationship: a novel method with potential for noninvasive application". In: *American Journal of Physiology-Heart and Circulatory Physiology* 291.1 (2006), H403–H412.

[37] Kimberly A Krabill et al. "Echocardiographic versus cardiac catheterization diagnosis of infants with congenital heart disease requiring cardiac surgery". In: *The American journal of cardiology* 60.4 (1987), pp. 351–354.

[38] Bonnie Ky et al. "Ventricular-arterial coupling, remodeling, and prognosis in chronic heart failure". In: *Journal of the American College of Cardiology* 62.13 (2013), pp. 1165–1172.

[39] GJ Langewouters, WJ Goedhard, and KH Wesseling. "The effect of aging and sclerosis on the viscoelastic properties of the human thoracic aorta". In: *Tijdschrift voor gerontologie en geriatrie* 16.2 (1985), pp. 61–70.

[40] GJ Langewouters, KH Wesseling, and WJA Goedhard. "The static elastic properties of 45 human thoracic and 20 abdominal aortas in vitro and the parameters of a new model". In: *Journal of biomechanics* 17.6 (1984), pp. 425–435.

[41] Dominic Y Leung et al. "Latent left ventricular dysfunction in patients with mitral regurgitation: feasibility of measuring diminished contractile reserve from a simplified model of noninvasively derived left ventricular pressure-volume loops". In: *American heart journal* 137.3 (1999), pp. 427–434.

[42] John K-J Li. "Arterial wall properties in men and women: Hemodynamic analysis and clinical implications". In: *Sex-Specific Analysis of Cardiovascular Function*. Springer, 2018, pp. 291–306.

[43] Zeng-Ding Liu et al. "Cuffless Blood Pressure Estimation Using Pressure Pulse Wave Signals". In: *Sensors* 18.12 (2018), p. 4227.

[44] Zhaorong Liu, Kenneth P Brin, and FC Yin. "Estimation of total arterial compliance: an improved method and evaluation of current methods". In: *American Journal of Physiology-Heart and Circulatory Physiology* 251.3 (1986), H588–H600.

[45] Maria Łoboz-Rudnicka et al. "gender-related differences in the progression of carotid stiffness with age and in the influence of risk factors on carotid stiffness". In: *Clinical interventions in aging* 13 (2018), p. 1183.

[46] AS Meidert, J Briegel, and B Saugel. "Principles and pitfalls of arterial blood pressure measurement". In: *Der Anaesthesist* (2019).

[47] Asako Miyaki et al. “Is pentraxin 3 involved in obesity-induced decrease in arterial distensibility?” In: *Journal of atherosclerosis and thrombosis* (2010), pp. 1002040175–1002040175.

[48] Neil E Moat et al. “Long-term outcomes after transcatheter aortic valve implantation in high-risk patients with severe aortic stenosis: the UK TAVI (United Kingdom Transcatheter Aortic Valve Implantation) Registry”. In: *Journal of the American College of Cardiology* 58.20 (2011), pp. 2130–2138.

[49] Edgar A Newfeld et al. “Discrete subvalvular aortic stenosis in childhood: study of 51 patients”. In: *The American journal of cardiology* 38.1 (1976), pp. 53–61.

[50] Vuyisile T Nkomo et al. “Burden of valvular heart diseases: a population-based study”. In: *The Lancet* 368.9540 (2006), pp. 1005–1011.

[51] Ruben LJ Osnabrugge et al. “Aortic stenosis in the elderly: disease prevalence and number of candidates for transcatheter aortic valve replacement: a meta-analysis and modeling study”. In: *Journal of the American College of Cardiology* 62.11 (2013), pp. 1002–1012.

[52] S Rastegar et al. “Estimating Systolic Blood Pressure Using Convolutional Neural Networks.” In: *Studies in health technology and informatics* 261 (2019), pp. 143–149.

[53] Alexander Reshetnik et al. “Validation of noninvasive oscillometric blood pressure 2020 up pressure upper arm blood pressure monitoring technology according to the European Society of Hypertension International Protocol revision 2010”. In: *Blood pressure monitoring* 24.2 (2019), pp. 99–101.

[54] Josep Rodés-Cabau et al. “Transcatheter aortic valve implantation for the treatment of severe symptomatic aortic stenosis in patients at very high or prohibitive surgical risk: acute and late outcomes of the multicenter Canadian experience”. In: *Journal of the American College of Cardiology* 55.11 (2010), pp. 1080–1090.

[55] Kiichi Sagawa. “Cardiovascular interaction”. In: *Cardiac contraction and the pressure-volume relationship* (1988).

[56] Kiichi Sagawa. “The ventricular pressure-volume diagram revisited.” In: *Circulation Research* 43.5 (1978), pp. 677–687.

[57] Ramsay MAE Scheeren TWL. “New Developments in Hemodynamic Monitoring”. In: *J Cardiothorac Vasc Anesth* 33 (2019), S67–S72.

[58] William M Schultz et al. “Socioeconomic status and cardiovascular outcomes: challenges and interventions”. In: *Circulation* 137.20 (2018), pp. 2166–2178.

[59] Patrick Segers et al. “Systemic and pulmonary hemodynamics assessed with a lumped-parameter heart-arterial interaction model”. In: *Journal of Engineering Mathematics* 47.3-4 (2003), pp. 185–199.

[60] Nandakumar Selvaraj and Hitesh Reddivari. “Feasibility of Noninvasive Blood Pressure Measurement using a Chest-worn Patch Sensor”. In: *2018 40th Annual International Conference of the IEEE Engineering in Medicine and Biology Society (EMBC)*. IEEE. 2018, pp. 1–4.

[61] Hideaki Senzaki, Chen-huan Chen, and David A Kass. “Valvular Heart Disease/heart Failure/hypertension: Single-beat Estimation of End-systolic Pressure-volume Relation in Humans”. In: *Circulation* 94.10 (1996), pp. 2497–2506.

[62] Toshiaki Shishido et al. “Single-beat estimation of end-systolic elastance using bilinearly approximated time-varying elastance curve”. In: *Circulation* 102.16 (2000), pp. 1983–1989.

[63] Hafize Emine Sönmez et al. “The Relationship between the Waist Circumference and Increased Carotid Intima Thickness in Obese Children”. In: *Childhood Obesity* (2019).

[64] Hidemi Sorimachi et al. “Sex differences in left ventricular afterload and diastolic function are independent from the aortic size”. In: *PloS one* 14.4 (2019), e0214907.

[65] Hiroyuki Suga. “Time course of left ventricular pressure-volume relationship under various enddiastolic volume”. In: *Japanese heart journal* 10.6 (1969), pp. 509–515.

[66] Hiroyuki Suga and Kiichi Sagawa. “Instantaneous pressure-volume relationships and their ratio in the excised, supported canine left ventricle”. In: *Circulation research* 35.1 (1974), pp. 117–126.

[67] Miho Sumiyoshi et al. “Accuracy of the ClearSight^{TM} system in patients undergoing abdominal aortic aneurysm surgery”. In: *Journal of anesthesia* (2019), pp. 1–8.

[68] Deepak R Talreja et al. “Constrictive pericarditis in the modern era: novel criteria for diagnosis in the cardiac catheterization laboratory”. In: *Journal of the American College of Cardiology* 51.3 (2008), pp. 315–319.

[69] Jeremy J Thaden, Vuyisile T Nkomo, and Maurice Enriquez-Sarano. “The global burden of aortic stenosis”. In: *Progress in cardiovascular diseases* 56.6 (2014), pp. 565–571.

[70] Sven AF Tulner et al. “Surgical ventricular restoration in patients with ischemic dilated cardiomyopathy: evaluation of systolic and diastolic ventricular function, wall stress, dyssynchrony, and mechanical efficiency by pressure-volume loops”. In: *The Journal of Thoracic and Cardiovascular Surgery* 132.3 (2006), pp. 610–620.

[71] Chonghe Wang et al. “Monitoring of the central blood pressure waveform via a conformal ultrasonic device”. In: *Nature biomedical engineering* 2.9 (2018), p. 687.

[72] Chinnadurai SK Watson MK. “Evaluation of noninvasive oscillometric blood pressure monitoring in anesthetized Bennett’s wallabies (Macropus rufogriseus)”. In: *J Zoo Wildl Med.* (2019), pp. 389–395.

[73] Heidi Weberruß et al. “Intima-media thickness and arterial function in obese and non-obese children”. In: *BMC obesity* 3.1 (2015), p. 2.

[74] Nico Westerhof, Jan-Willem Lankhaar, and Berend E Westerhof. “The arterial windkessel”. In: *Medical & biological engineering & computing* 47.2 (2009), pp. 131–141.

[75] Erik Wetterer. *Quantitative Beziehungen zwischen Stromstärke und Druck im natürlichen Kreislauf bei zeitlich variabler Elastizität des arteriellen Windkessels; Wetterer, Erik, Dr. med*. JF Lehmanns Verlag, 1940.

[76] Floris L Wuyts et al. “Elastic properties of human aortas in relation to age and atherosclerosis: a structural model”. In: *Physics in Medicine & Biology* 40.10 (1995), p. 1577.

[77] Xiaoman Xing et al. "An Unobtrusive and Calibration-free Blood pressure estimation Method using photoplethysmography and Biometrics". In: *Scientific reports* 9.1 (2019), p. 8611.

[78] Yang Yao et al. "Unobtrusive Estimation of Cardiovascular Parameters with Limb Ballistocardiography". In: *Sensors* 19.13 (2019), p. 2922.

[79] Masashi Yokose et al. "The perfusion index measured by the pulse oximeter affects the agreement between ClearSight and the arterial catheter-based blood pressures: A prospective observational study". In: *PloS one* 14.7 (2019), e0219511.